**RBP-J regulates homeostasis and function of circulating Ly6C$^{lo}$ monocytes**

Tiantian Kou[1,2,3,6], Lan Kang[1,3,6], Bin Zhang[1,3], Jiaqi Li[1], Baohong Zhao[4,5], Wenwen Zeng[1,2,3], Xiaoyu Hu[1,2,3,*]

**Affiliations:**

[1]Institute for Immunology and School of Medicine, Tsinghua University, Beijing, China.

[2]Tsinghua-Peking Center for Life Sciences, Tsinghua University, Beijing, China.

[3]Beijing Key Laboratory for Immunological Research on Chronic Diseases, Beijing, China.

[4]Arthritis and Tissue Degeneration Program and the David Z. Rosensweig Genomics Research Center, Hospital for Special Surgery, New York, NY.

[5]Department of Medicine, Weill Cornell Medicine, New York, NY.

[6]These authors contributed equally.

[*]Correspondence: xiaoyuhu@tsinghua.edu.cn.

**Abstract**

Notch-RBP-J signaling plays an essential role in maintenance of myeloid homeostasis. However, its role in monocyte cell fate decisions is not fully understood. Here we showed that conditional deletion of transcription factor RBP-J in myeloid cells resulted in marked accumulation of blood Ly6C$^{lo}$ monocytes that highly expressed chemokine receptor CCR2. Bone marrow transplantation and parabiosis experiments revealed a cell intrinsic requirement of RBP-J for controlling blood Ly6C$^{lo}$CCR2$^{hi}$ monocytes. RBP-J-deficient Ly6C$^{lo}$ monocytes exhibited enhanced capacity competing with wildtype counterparts in blood circulation. In accordance with alterations of circulating monocytes, RBP-J deficiency led to markedly increased population of lung tissues with Ly6C$^{lo}$ monocytes and CD16.2$^{+}$ interstitial macrophages. Furthermore, RBP-J deficiency-associated phenotypes could be genetically corrected by further deleting *Ccr2* in myeloid cells. These results demonstrate that RBP-J functions as a crucial regulator of blood Ly6C$^{lo}$ monocytes and thus derived lung-resident myeloid populations, at least in part through regulation of CCR2.

**Key words:**

RBP-J; Ly6C$^{lo}$ monocyte; CCR2; Lung interstitial macrophage

## Introduction

Monocytes are integral components of the mononuclear phagocyte system (MPS) that develop from monocyte precursors in the bone marrow(Guilliams et al., 2018). Several functionally and phenotypically distinct subsets of blood monocytes have been defined on the basis of expression of surface markers(Cros et al., 2010; Geissmann et al., 2003; Passlick et al., 1989; Weber et al., 2000). In mice, Ly6C$^{hi}$ monocytes (also called inflammatory or classical monocytes) characterized by Ly6C$^{hi}$CCR2$^{hi}$CX3CR1$^{lo}$ exhibit a short half-life, and are recruited to tissue and differentiate into macrophages and dendritic cells(Ginhoux and Jung, 2014). Ly6C$^{hi}$ monocytes are analogous to CD14$^{+}$ human monocytes based on gene expression profiling(Ingersoll et al., 2010). A second subtype of monocytes is called Ly6C$^{lo}$ monocytes (also termed patrolling monocytes or non-classical monocytes), which express high level of CX3CR1 and low level of CCR2, equivalent to CD14$^{lo}$CD16$^{+}$ human monocytes. Ly6C$^{lo}$ monocytes are regarded as blood-resident macrophages that patrol blood vessels and scavenge microparticles attached to the endothelium under physiological conditions, and exhibit a long half-life in the steady-state(Auffray et al., 2007; Carlin et al., 2013; Yona et al., 2013). Ly6C$^{lo}$ monocytes may exert a protective effect by suppressing atherosclerosis in mice, while high levels of non-classical monocytes have been associated with more advanced vascular dysfunction and oxidative stress in patients with coronary artery disease(Hamers et al., 2012; Hanna et al., 2012; Urbanski et al., 2017). In the inflammatory settings, Ly6C$^{lo}$ monocytes often show anti-inflammatory properties, yet also exhibit a proinflammatory role under certain circumstances(Amano et al., 2005; Brunet et al., 2016; Carlin et al., 2013; Cros et al., 2010; Misharin et al., 2014; Nahrendorf et al., 2007; Puchner et al., 2018). In addition, Ly6C$^{lo}$ monocytes have demonstrated protective functions in tumorigenesis, such as engulfing tumor materials to prevent cancer metastasis, activating and recruiting NK cells to the lungs(Hanna et al., 2015; Thomas et al., 2016). While the functions of Ly6C$^{lo}$ monocytes are complex and sometimes contradictory depending on the animal models and experimental approaches, it is clear that they play a crucial role in both health and disease.

The generation and maintenance of Ly6C$^{lo}$ monocytes are regulated by several transcription factors, including Nr4a1 and CEBPβ(Hanna et al., 2011; Tamura et al., 2017). The colony-stimulating factor 1 receptor (CSF1R) signaling pathway is important for the generation and survival of Ly6C$^{lo}$ monocytes, and neutralizing antibodies against CSF1R can reduce their numbers(MacDonald et al., 2010). Interestingly, recent studies have suggested that different subsets of monocytes may be supported by distinct cellular sources of CSF-1 within bone marrow niches, in which targeted deletion of *Csf1* from sinusoidal endothelial cells selectively reduces Ly6C$^{lo}$ monocytes but not Ly6C$^{hi}$ monocytes(Emoto et al., 2022). LAIR1 has been shown to be activated by stromal protein Colec12, and LAIR1 deficiency leads to aberrant proliferation and apoptosis in bone marrow non-classical monocytes(Keerthivasan et al., 2021). These findings further underscore the complexity of the mechanisms that regulate Ly6C$^{lo}$ monocytes, and suggest that multiple factors are involved in this process.

Recombination signal-binding protein for immunoglobulin kappa J region (RBP-J; also named CSL in humans) is commonly known as the master nuclear mediator of canonical Notch signaling(Radtke et al., 2013). In the absence of Notch intracellular domain, RBP-J associates with co-repressor proteins to repress transcription of downstream target genes. In the immune system, the best studied functions of Notch signaling are its roles in regulating the development of lymphocytes, such as T cells and marginal zone B cells(Radtke et al., 2013). Notch signaling also has been reported to regulate the differentiation and function of myeloid cells including granulocyte/monocyte progenitors, osteoclasts and dendritic cells (Caton et al., 2007; Klinakis et al., 2011; Lewis et al., 2011; Zhao et al., 2012). In osteoclasts, RBP-J represses osteoclastogenesis, particularly under inflammatory conditions(Zhao et al., 2012). In dendritic cells, Notch-RBP-J signaling controls the maintenance of CD8$^{-}$ DC(Caton et al., 2007). In addition, Notch2-RBP-J pathway is essential for development of CD8$^{-}$ESAM$^{+}$ DC in the spleen and CD103$^{+}$CD11b$^{+}$ DC in the lamina propria of the intestine(Lewis et al., 2011). However, the role of Notch-RBP-J signaling

pathway in regulating monocyte subsets remains elusive. Here, we demonstrated that RBP-J controlled homeostasis of blood Ly6C$^{lo}$ monocytes in a cell intrinsic manner. RBP-J deficiency led to a drastic increase in blood Ly6C$^{lo}$ monocytes, lung Ly6C$^{lo}$ monocytes and CD16.2$^{+}$ IM. Our results suggest that RBP-J plays a critical role in regulating the population and characteristics of Ly6C$^{lo}$ monocytes in the blood and lung.

## Results

### RBP-J is essential for maintenance of blood Ly6C$^{lo}$ monocytes

To investigate the role of RBP-J in monocyte subsets, we utilized mice with RBP-J specific deletion in the myeloid cells (*Rbpj*$^{fl/fl}$*Lyz2*$^{cre/cre}$ mice). Efficient deletion of *Rbpj* in blood monocytes was confirmed by quantitative real-time PCR (qPCR) (Figure 1 - figure supplement 1A). Flow cytometric analysis revealed that RBP-J deficient mice had a significant increase in the proportion of Ly6C$^{lo}$ monocytes, but not Ly6C$^{hi}$ monocytes, in blood, compared to age-matched control mice with the genotype *Rbpj*$^{+/+}$*Lyz2*$^{cre/cre}$ (Figure 1A). In contrast to circulating monocytes, RBP-J deficient mice exhibited minimal alterations in the percentages of monocyte subsets in bone marrow (BM) and spleen (Figure 1B and Figure 1 - figure supplement 1C). Additionally, RBP-J deficiency in myeloid cells did not appear to have an effect on neutrophils (Figure 1- figure supplement 1B). Therefore, among circulating myeloid populations, RBP-J selectively controlled the subset of Ly6C$^{lo}$ monocytes.

BM progenitors that give rise to circulating monocytes are monocyte-dendritic cell progenitors (MDPs) and common monocyte progenitors (cMoPs)(Hanna et al., 2011; Hettinger et al., 2013; Liu et al., 2019; Varol et al., 2007). Next, we analyzed BM progenitors, and found that the percentages of MDPs and cMoPs were equivalent in control and RBP-J deficient mice (Figure 1C). These results in conjunction with the observations of normal BM monocyte populations suggest that alterations of peripheral blood Ly6C$^{lo}$ monocytes may not originate from BM. Next, we examined whether RBP-J may influence the egress of Ly6C$^{lo}$ monocytes from BM, and measured BM exit rate of Ly6C$^{lo}$ monocytes using *in vivo* labeling of sinusoidal cells as previously described

(Figure 1D)(Debien et al., 2013). The results showed that RBP-J deficiency did not
135 affect egress of Ly6C$^{lo}$ monocytes from BM (Figure 1E). Taken together, these data revealed RBP-J as a critical regulator controlling homeostasis of peripheral blood Ly6C$^{lo}$ monocytes.

**RBP-J deficiency does not affect Ly6C$^{hi}$ monocyte conversion or Ly6C$^{lo}$ monocyte**
140 **survival and proliferation**

Next, we aimed to determine whether the increase of blood Ly6C$^{lo}$ monocytes in RBP-J deficient mice was due to decreased cell death or enhanced proliferation. We first stained monocytes with Annexin V and 7-AAD to identify apoptotic cells and observed comparable percentages of apoptotic blood Ly6C$^{lo}$ monocytes in control and RBP-J
145 deficient mice (Figure 2A). Given the crucial role of Nr4a1 in the survival of Ly6C$^{lo}$ monocytes(Hanna et al., 2011), we detected the expression of Nr4a1, which was similar in Ly6C$^{lo}$ monocytes from control and RBP-J deficient mice (Figure 2- figure supplement 1A). We then assessed the proliferative capacity by analyzing Ki-67 expression as well as *in vivo* EdU incorporation. Ki-67 levels in blood monocytes
150 displayed no differences between control and RBP-J deficient mice (Figure 2B). The percentage of EdU$^{+}$ monocytes did not significantly differ between control and RBP-J deficient mice at the indicated time points, implying that the turnover of Ly6C$^{lo}$ monocytes was normal in RBP-J deficient mice (Figure 2C). Fluorescent latex beads as particulate tracers could be phagocytosed by monocytes after intravenous injection, and
155 stably label Ly6C$^{lo}$ monocytes(Tacke et al., 2006). Thus, we intravenously injected fluorescent latex beads into control and RBP-J deficient mice to track circulating monocytes (Figure 2D). By day 7 post injection, only Ly6C$^{lo}$ monocytes were latex$^{+}$ as previously reported(Tacke et al., 2006), whereas control and RBP-J deficient mice groups presented a similar frequency of latex$^{+}$ monocytes (Figure 2E). Together, these
160 data indicated that RBP-J did not influence monocyte survival and proliferation.

Previous studies have shown that Ly6C$^{lo}$ monocytes are observed in recipient mice following the adoptive transfer of Ly6C$^{hi}$ monocytes, indicating that Ly6C$^{hi}$ monocytes

can convert into Ly6C$^{lo}$ monocytes(Varol et al., 2007; Yona et al., 2013). We next wished to evaluate whether conversion of Ly6C$^{hi}$ monocyte was regulated by RBP-J by isolating bone marrow GFP$^{+}$Ly6C$^{hi}$ monocytes from *Lyz2*$^{cre/cre}$*Cx3cr1*$^{gfp/+}$ control or *Rbpj*$^{fl/fl}$*Lyz2*$^{cre/cre}$*Cx3cr1*$^{gfp/+}$ mice and adoptively transferring them into *Ccr2*$^{RFP/RFP}$ recipients (Figure 2F). Sixty hours after transfer, a subset of cells from donors were converted into Ly6C$^{lo}$ monocytes (Figure 2 - figure supplement 1B), and equal percentages of Ly6C$^{lo}$ monocytes were derived from control and *Rbpj*$^{fl/fl}$*Lyz2*$^{cre/cre}$*Cx3cr1*$^{gfp/+}$ donors (Figure 2G). Thus, the conversion of Ly6C$^{hi}$ monocyte into Ly6C$^{lo}$ monocyte was not affected by RBP-J deficiency.

**RBP-J regulates blood Ly6C$^{lo}$ monocytes in a cell intrinsic manner**

We next wondered whether the increase of Ly6C$^{lo}$ monocytes in RBP-J deficient mice was bone marrow-derived and cell intrinsic. We performed bone marrow transplantation by engrafting lethally irradiated mice with a 1:4 mixture of *Rbpj*$^{+/+}$*Lyz2*$^{cre/cre}$ control and *Rbpj*$^{fl/fl}$*Lyz2*$^{cre/cre}$ BM cells (CD45.2) and *Cx3cr1*$^{gfp/+}$ BM cells (CD45.1) (Figure 3A). Eight weeks after transplantation, we analyzed the frequencies of CD45.2$^{+}$ donor cells in the bone marrow and blood of recipient mice and found that the frequencies of CD45.2$^{+}$ cells within total cells were similar to the mixture ratio of bone marrow cells for Ly6C$^{hi}$ monocytes and neutrophils in both BM and blood (Figure 3B and Figure 3 - figure supplement 1A and B). Specifically, more blood Ly6C$^{lo}$ monocytes were derived from RBP-J deficient donors than control donors (Figure 3B), reflecting that the contribution of RBP-J deficient cells in blood Ly6C$^{lo}$ cells was significantly higher than that of control cells. These results implied that RBP-J deficient BM cells were highly efficient in generating blood Ly6C$^{lo}$ monocytes.

Given that RBP-J deficient mice had more Ly6C$^{lo}$ monocytes in blood than did control mice, we performed parabiosis experiments, a surgical union of two organisms, which allowed parabiotic mice to share their blood circulation. The contribution of circulating cells from one animal in another can be estimated by measuring the percentage of blood cells that originated from each animal(Liu et al., 2007). We joined

a CD45.1, *Cx3cr1*$^{gfp/+}$ mouse with an age and sex-matched *Rbpj*$^{+/+}$*Lyz2*$^{cre/cre}$ control or
195 *Rbpj*$^{fl/fl}$*Lyz2*$^{cre/cre}$ mouse (CD45.2) (Figure 3C). Four weeks after the procedure, about 50% of B cells and T cells in parabiotic mice displayed efficient exchange of their circulation (Figure 3 - figure supplement 1C). As expected, RBP-J deficient mice exhibited higher percentages of Ly6C$^{lo}$ monocytes than control animals (Figure 3D). Intriguingly, in the parabiotic *Cx3cr1*$^{gfp/+}$ mice, RBP-J deficient cells still constituted
200 significantly higher proportion of circulating Ly6C$^{lo}$, but not Ly6C$^{hi}$ monocytes, than RBP-J sufficient counterparts as indicated by the percentages of the GFP-negative population (Figure 3E). These results implicated that the enhanced ability of Ly6C$^{lo}$ monocytes to circulate in the peripheral blood as a result of RBP-J deficiency was cell intrinsic.

205

**RBP-J regulates phenotypical marker genes in blood Ly6C$^{lo}$ monocytes**

To further study the consequences of RBP-J loss of function in blood Ly6C$^{lo}$ monocytes, we performed gene expression profiling by RNA-seq, which revealed that Ly6C$^{lo}$ monocytes in RBP-J deficient mice exhibited low expression of *Itgax* but high
210 expression of *Ccr2*, in comparison to those in control mice (Figure 4A). These differential expression patterns of phenotypic marker genes were also confirmed by qPCR and flow cytometry analysis (Figure 4B). However, Ly6C$^{hi}$ blood monocytes and BM monocytes displayed normal levels of CD11c and CCR2 (Figure 4B and Figure 4 - figure supplement 1A). Moreover, principal component analysis showed distinct
215 expression pattern of monocytes between control and RBP-J deficient mice (Figure 4C). To determine whether the regulation of phenotypic markers by RBP-J in blood Ly6C$^{lo}$ monocytes was cell-intrinsic, we performed BM transplantation as described above (Figure 3A). The findings indicated that Ly6C$^{lo}$ monocytes derived from RBP-J deficient BM cells expressed high levels of CCR2 but low levels of CD11c, in
220 comparison to those derived from control BM cells, whereas no significant changes were observed in blood Ly6C$^{hi}$ and BM monocytes, as expected (Figure 4D and Figure 4 - figure supplement 1B). These results collectively suggested that RBP-J regulated the expression of CCR2/CD11c in a cell-intrinsic manner.

225 **RBP-J-mediated control of blood Ly6C$^{lo}$ monocytes is CCR2 dependent**

Given that RBP-J deficiency led to enhanced CCR2 expression in Ly6C$^{lo}$ monocytes and that CCR2 is essential for monocyte functionality under various inflammatory and non-inflammatory conditions(Shi and Pamer, 2011), we wished to genetically investigate the role of CCR2 in the RBP-J deficient background. We generated RBP-
230 J/CCR2 double deficient (DKO) mice with the genotype *Rbpj*$^{fl/fl}$*Lyz2*$^{cre/cre}$*Ccr2*$^{RFP/RFP}$ with *Lyz2*$^{cre/cre}$*Ccr2*$^{RFP/+}$ and *Rbpj*$^{fl/fl}$*Lyz2*$^{cre/cre}$*Ccr2*$^{RFP/+}$ mice serving as controls. As expected, the expression of CCR2 in Ly6C$^{lo}$ monocytes was reduced in DKO mice compared to RBP-J deficient mice (Figure 5A), confirming the successful deletion of the *Ccr2* gene. DKO mice showed a lower percentage of both Ly6C$^{hi}$ and Ly6C$^{lo}$
235 monocytes than RBP-J deficient mice (Figure 5B and C). Notably, the percentage of Ly6C$^{lo}$ monocytes in DKO mice was comparable to that observed in the control mice (Figure 5B and C), implicating that deletion of CCR2 corrected RBP-J deficiency-associated phenotype of increased Ly6C$^{lo}$ monocytes. Whereas, both RBP-J deficient and DKO mice exhibited lower expression levels of CD11c in their Ly6C$^{lo}$ monocyte
240 than control mice, suggesting that the regulation of CD11c expression was independent of CCR2 (Figure 5D). These results suggested that RBP-J regulated Ly6C$^{lo}$ monocytes, at least in part, through CCR2.

**Lung Ly6C$^{lo}$ monocytes are accumulated in RBP-J deficient mice**

245 In mice, alveolar macrophages (AM) are maintained by local self-renewal, and arise from fetal liver derived precursors, whereas interstitial macrophages (IM) are probably originated from monocytes (Guilliams et al., 2013; Hashimoto et al., 2013; Sabatel et al., 2017). Schyns et al identified 3 subpopulations of IM according to expression of CD206 and CD16.2 and Ly6C$^{lo}$ monocytes are proposed to give rise to CD64$^{+}$CD16.2$^{+}$
250 IM(Schyns et al., 2019). We next compared the populations of lung monocytes and IM between control and RBP-J deficient mice. The conditional deletion of RBP-J resulted in a significant increase in the absolute and relative numbers of Ly6C$^{lo}$ monocytes and CD16.2$^{+}$ IM, while the numbers of Ly6C$^{hi}$ monocytes, CD206$^{-}$ IM, and CD206$^{+}$ IM

remained unchanged (Figure 6A and B). To confirm these findings, lung sections from
255 *Lyz2*$^{cre/cre}$*Cx3cr1*$^{gfp/+}$ control and *Rbpj*$^{fl/fl}$*Lyz2*$^{cre/cre}$*Cx3cr1*$^{gfp/+}$ mice were stained with an anti-GFP antibody, which revealed a significant increase in the number of GFP$^{+}$ cells in RBP-J deficient mice (Figure 6C). In addition, we evaluated the proliferative capacity of Ly6C$^{lo}$ monocytes and CD16.2$^{+}$ IM, but did not observe enhanced EdU incorporation in Ly6C$^{lo}$ monocytes and CD16.2$^{+}$ IM from RBP-J deficient mice (Figure 6 - figure
260 supplement 1A and B). These findings suggested that the augmented population of these cells might not be resulted from increased *in situ* proliferation. Previous reports have indicated that LPS can increase the population of IM in a CCR2-dependent manner(Sabatel et al., 2017). We thus challenged mice with LPS, and analyzed monocytes and IM at day 0 and day 4. LPS exposure induced an increase in numbers
265 of Ly6C$^{lo}$ monocytes, CD16.2$^{+}$ IM and CD206$^{-}$ IM compared to baseline both in control and RBP-J deficient mice (Figure 6D and E). There was a trend toward higher Ly6C$^{hi}$ monocyte after LPS treatment, although this observation was not statistically significant. Of note, RBP-J deficient mice exhibited robustly elevated numbers of Ly6C$^{lo}$ monocytes and CD16.2$^{+}$ IM compared with control mice after LPS treatment (Figure
270 6D and E), suggesting that RBP-J deficient Ly6C$^{lo}$ monocytes were recruited to inflamed tissue in large numbers and differentiated into CD16.2$^{+}$ IM.

To investigate whether the elevated levels of lung monocytes and CD16.2$^{+}$ IM in RBP-J deficient mice were derived from blood Ly6C$^{lo}$ monocytes, we examined
275 monocytes and IM in *Lyz2*$^{cre/cre}$*Ccr2*$^{RFP/+}$ control, *Lyz2*$^{cre/cre}$*Ccr2*$^{RFP/RFP}$, *Rbpj*$^{fl/fl}$*Lyz2*$^{cre/cre}$*Ccr2*$^{RFP/+}$, and *Rbpj*$^{fl/fl}$*Lyz2*$^{cre/cre}$*Ccr2*$^{RFP/RFP}$ (DKO) mice. The deletion of CCR2 led to a decrease in Ly6C$^{hi}$ monocytes, and the Ly6C$^{lo}$ monocytes in DKO mice were reduced to a level similar to that of control mice (Figure 7A and B). While the DKO mice had more CD16.2$^{+}$ IM compared to control mice, these cells were
280 severely reduced compared to RBP-J deficient mice (Figure 7A and C). The above data supported the notion that increased lung Ly6C$^{lo}$ monocytes and CD16.2$^{+}$ IM in RBP-J deficient mice were derived from Ly6C$^{lo}$ blood monocytes. In summary, these results suggested that in RBP-J deficient mice, recruitment of blood Ly6C$^{lo}$ monocytes to the

lung was markedly facilitated by increased cell number as well as heightened expression of CCR2, leading to the increase of lung Ly6C$^{lo}$ monocytes and CD16.2$^{+}$ IM.

**Discussion**

In this study, we identified RBP-J as a pivotal factor in regulating blood Ly6C$^{lo}$ monocyte cell fate. Our results showed that mice with conditional deletion of RBP-J in myeloid cells exhibited a robust increase in blood Ly6C$^{lo}$ monocytes, and subsequently accumulated lung Ly6C$^{lo}$ monocytes and CD16.2$^{+}$ IM under steady-state conditions. Bone marrow transplantation experiments in which RBP-J deficient cells were transplanted into recipient mice as well as the parabiosis experiment showed similar increase in blood Ly6C$^{lo}$ monocytes, demonstrating that RBP-J was an intrinsic factor required for the regulation of Ly6C$^{lo}$ monocytes. Further analysis revealed that RBP-J regulated the expression of CCR2 and CD11c on the surface of Ly6C$^{lo}$ monocytes. Moreover, the phenotype of elevated blood Ly6C$^{lo}$ monocytes and their progeny was further ameliorated by deleting *Ccr2* in a RBP-J deficient background.

Notch-RBP-J signaling has been shown to play a role in regulating functional polarization and activation of macrophages, and regulated formation of Kupffer cells and macrophage differentiation from Ly6C$^{hi}$ monocytes in ischemia(Foldi et al., 2016; Hu et al., 2008; Kang et al., 2020; Krishnasamy et al., 2017; Sakai et al., 2019; Wang et al., 2010; Xu et al., 2012). At steady-state, interaction of DLL1 with Notch 2 regulates conversion of Ly6C$^{hi}$ monocytes into Ly6C$^{lo}$ monocytes in special niches of the BM and spleen(Gamrekelashvili et al., 2016). Under inflammatory conditions, Notch2 and TLR7 pathways independently and synergistically promote conversion of Ly6C$^{hi}$ monocytes into Ly6C$^{lo}$ monocytes(Gamrekelashvili et al., 2020). However, in our study, the percentage of blood Ly6C$^{lo}$ monocytes increased in RBP-J deficient mice. These results somewhat differ from what was observed in mice with conditional deletion of Notch2(Gamrekelashvili et al., 2016). Actually, 4 members of the Notch family have been identified in mammals(Radtke et al., 2013). Thus, Notch receptors seem to be non-

redundant in regulating monocyte cell fate, and distinct Notch receptors are likely to
315 act in a concerted manner to coordinate the monocyte differentiation program.

Colony-stimulating factor 1 receptor (CSF1R) signal, CX3CR1, CEBPβ and Nr4a1 have been suggested to be involved in the generation and survival of Ly6C$^{lo}$ monocytes. The lifespan of Ly6C$^{lo}$ monocytes is acutely shortened after blockade of CSF1R, and
320 the numbers of these cells are reduced, and the percentage of dead cells increased in mice with endothelial cell-specific depletion of *Csf1*(Emoto et al., 2022; MacDonald et al., 2010). CX3CR1 and CEBPβ-knockout mice show accelerated death of Ly6C$^{lo}$ monocyte, display the decreased level of Ly6C$^{lo}$ monocytes(Landsman et al., 2009; Tamura et al., 2017). Nr4a1 knockout mice have significantly fewer monocytes in blood,
325 bone marrow, and spleen, due to differentiation deficiency in MDP and accelerated apoptosis of Ly6C$^{lo}$ monocytes in bone marrow(Hanna et al., 2011). RBP-J deficient mice had normal MDP and Ly6C$^{lo}$ monocytes, expressed normal level of Nr4a1 and Ki-67, exhibited normal half-life and turnover rate, which suggested that RBP-J may not regulate Ly6C$^{lo}$ monocytes through these factors. Further studies are required to
330 elucidate the precise molecular mechanisms of RBP-J in Ly6C$^{lo}$ monocytes under steady state.

At the steady state, Ly6C$^{lo}$ monocytes patrol endothelium of blood vessel. After R848 induced endothelial injury, Ly6C$^{lo}$ monocytes recruit neutrophils to mediate focal
335 endothelial necrosis and fuel vascular inflammation, and subsequently, the Ly6C$^{lo}$ monocytes remove cellular debris(Carlin et al., 2013; Imhof et al., 2016). In response to *Listeria monocytogenes* infection, Ly6C$^{lo}$ monocytes can extravasate but do not give rise to macrophages or DCs(Auffray et al., 2007). Additional evidence shows that Ly6C$^{lo}$ monocytes do not merely act as luminal blood macrophages. In lung, exposure
340 to unmethylated CpG DNA expands CD16.2$^{+}$ IM, which originate from Ly6C$^{lo}$ monocytes and spontaneously produce IL-10, thereby preventing allergic inflammation(Schyns et al., 2019). A recent study shows that Ly6C$^{lo}$ monocytes give rise to CD9$^{+}$ macrophages, which provide an intracellular replication niche for

*Salmonella* Typhimurium in spleen, and Ly6C$^{lo}$-depleted mice are more resistant to *Salmonella* Typhimurium infection, suggesting that Ly6C$^{lo}$ monocytes exert certain functions in systemic infection(Hoffman et al., 2021). Our data provide evidence for RBP-J in the function of blood Ly6C$^{lo}$ monocytes, as RBP-J deficient Ly6C$^{lo}$ monocytes exhibited enhanced competition in blood circulation, as well as gave rise to increased numbers of lung CD16.2$^{+}$ IM. In summary, we showed that RBP-J acted as a fundamental regulator of the maintenance of blood Ly6C$^{lo}$ monocytes and their descendent, at least in part through regulation of CCR2. These results provide insights into understanding the mechanisms that regulate monocyte homeostasis and function.

## References


Amano, H., E. Amano, M.L. Santiago-Raber, T. Moll, E. Martinez-Soria, L. Fossati-Jimack, M. Iwamoto, S.J. Rozzo, B.L. Kotzin, and S. Izui. 2005. Selective expansion of a monocyte subset expressing the CD11c dendritic cell marker in the Yaa model of systemic lupus erythematosus. *Arthritis Rheum* 52:2790-2798. 10.1002/art.21365.

Auffray, C., D. Fogg, M. Garfa, G. Elain, O. Join-Lambert, S. Kayal, S. Sarnacki, A. Cumano, G. Lauvau, and F. Geissmann. 2007. Monitoring of blood vessels and tissues by a population of monocytes with patrolling behavior. *Science* 317:666-670. 10.1126/science.1142883.

Brunet, A., M. LeBel, B. Egarnes, C. Paquet-Bouchard, A.J. Lessard, J.P. Brown, and J. Gosselin. 2016. NR4A1-dependent Ly6C(low) monocytes contribute to reducing joint inflammation in arthritic mice through Treg cells. *Eur J Immunol* 46:2789-2800. 10.1002/eji.201646406.

Carlin, L.M., E.G. Stamatiades, C. Auffray, R.N. Hanna, L. Glover, G. Vizcay-Barrena, C.C. Hedrick, H.T. Cook, S. Diebold, and F. Geissmann. 2013. Nr4a1-dependent Ly6C(low) monocytes monitor endothelial cells and orchestrate their disposal. *Cell* 153:362-375. 10.1016/j.cell.2013.03.010.

Caton, M.L., M.R. Smith-Raska, and B. Reizis. 2007. Notch-RBP-J signaling controls the homeostasis of CD8- dendritic cells in the spleen. *J Exp Med* 204:1653-1664. 10.1084/jem.20062648.

Cros, J., N. Cagnard, K. Woollard, N. Patey, S.Y. Zhang, B. Senechal, A. Puel, S.K. Biswas, D. Moshous, C. Picard, J.P. Jais, D. D'Cruz, J.L. Casanova, C. Trouillet, and F. Geissmann. 2010. Human CD14dim monocytes patrol and sense nucleic acids and viruses via TLR7 and TLR8 receptors. *Immunity* 33:375-386. 10.1016/j.immuni.2010.08.012.

Debien, E., K. Mayol, V. Biajoux, C. Daussy, M.G. De Aguero, M. Taillardet, N. Dagany, L. Brinza, T. Henry, B. Dubois, D. Kaiserlian, J. Marvel, K. Balabanian, and T. Walzer. 2013. S1PR5 is pivotal for the homeostasis of patrolling monocytes. *Eur J Immunol* 43:1667-1675. 10.1002/eji.201343312.

Emoto, T., J. Lu, T. Sivasubramaniyam, H. Maan, A.B. Khan, A.A. Abow, S.A. Schroer, S.J. Hyduk, M.G. Althagafi, T.D. McKee, F. Fu, S. Shabro, A. Ulndreaj, F. Chiu, E. Paneda, S. Pacheco, T. Wang, A. Li, J.X. Jiang, P. Libby, et al. 2022. Colony stimulating factor-1 producing endothelial cells and mesenchymal stromal cells maintain monocytes within a perivascular bone marrow niche. *Immunity* 55:862-878 e868. 10.1016/j.immuni.2022.04.005.

Foldi, J., Y. Shang, B. Zhao, L.B. Ivashkiv, and X. Hu. 2016. RBP-J is required for M2 macrophage polarization in response to chitin and mediates expression of a subset of M2 genes. *Protein Cell* 7:201-209. 10.1007/s13238-016-0248-7.

Gamrekelashvili, J., R. Giagnorio, J. Jussofie, O. Soehnlein, J. Duchene, C.G. Briseno, S.K. Ramasamy, K. Krishnasamy, A. Limbourg, T. Kapanadze, C. Ishifune, R. Hinkel, F. Radtke, L.J. Strobl, U. Zimber-Strobl, L.C. Napp, J. Bauersachs, H. Haller, K. Yasutomo, C. Kupatt, et al. 2016. Regulation of monocyte cell fate by blood vessels mediated by Notch signalling. *Nat Commun* 7:12597. 10.1038/ncomms12597.

Gamrekelashvili, J., T. Kapanadze, S. Sablotny, C. Ratiu, K. Dastagir, M. Lochner, S. Karbach, P. Wenzel, A. Sitnow, S. Fleig, T. Sparwasser, U. Kalinke, B. Holzmann, H. Haller, and F.P. Limbourg. 2020. Notch and TLR signaling coordinate monocyte cell fate and inflammation. *Elife* 9:10.7554/eLife.57007.

Geissmann, F., S. Jung, and D.R. Littman. 2003. Blood Monocytes Consist of Two Principal Subsets with Distinct Migratory Properties. *Immunity* 19:71-82. 10.1016/s1074-7613(03)00174-2.

Ginhoux, F., and S. Jung. 2014. Monocytes and macrophages: developmental pathways and tissue homeostasis. *Nat Rev Immunol* 14:392-404. 10.1038/nri3671.

Guilliams, M., I. De Kleer, S. Henri, S. Post, L. Vanhoutte, S. De Prijck, K. Deswarte, B. Malissen, H. Hammad, and B.N. Lambrecht. 2013. Alveolar macrophages develop from fetal monocytes that differentiate into long-lived cells in the first week of life via GM-CSF. *J Exp Med* 210:1977-1992. 10.1084/jem.20131199.

Guilliams, M., A. Mildner, and S. Yona. 2018. Developmental and Functional Heterogeneity of Monocytes. *Immunity* 49:595-613. 10.1016/j.immuni.2018.10.005.

Hamers, A.A., M. Vos, F. Rassam, G. Marinkovic, K. Kurakula, P.J. van Gorp, M.P. de Winther, M.J. Gijbels, V. de Waard, and C.J. de Vries. 2012. Bone marrow-specific deficiency of nuclear receptor Nur77 enhances atherosclerosis. *Circ Res* 110:428-438. 10.1161/CIRCRESAHA.111.260760.

Hanna, R.N., L.M. Carlin, H.G. Hubbeling, D. Nackiewicz, A.M. Green, J.A. Punt, F. Geissmann, and C.C. Hedrick. 2011. The transcription factor NR4A1 (Nur77) controls bone marrow differentiation and the survival of Ly6C- monocytes. *Nat Immunol* 12:778-785. 10.1038/ni.2063.

Hanna, R.N., C. Cekic, D. Sag, R. Tacke, G.D. Thomas, H. Nowyhed, E. Herrley, N. Rasquinha, S. McArdle, R. Wu, E. Peluso, D. Metzger, H. Ichinose, I. Shaked, G. Chodaczek, S.K. Biswas, and C.C. Hedrick. 2015. Patrolling monocytes control tumor metastasis to the lung. *Science* 350:985-990. 10.1126/science.aac9407.

Hanna, R.N., I. Shaked, H.G. Hubbeling, J.A. Punt, R. Wu, E. Herrley, C. Zaugg, H. Pei, F. Geissmann, K. Ley, and C.C. Hedrick. 2012. NR4A1 (Nur77) deletion polarizes macrophages toward an inflammatory phenotype and increases atherosclerosis. *Circ Res* 110:416-427. 10.1161/CIRCRESAHA.111.253377.

Hashimoto, D., A. Chow, C. Noizat, P. Teo, M.B. Beasley, M. Leboeuf, C.D. Becker, P. See, J. Price, D. Lucas, M. Greter, A. Mortha, S.W. Boyer, E.C. Forsberg, M. Tanaka, N. van Rooijen, A. Garcia-Sastre, E.R. Stanley, F. Ginhoux, P.S. Frenette, et al. 2013. Tissue-resident macrophages self-maintain locally throughout adult life with minimal contribution from circulating monocytes. *Immunity* 38:792-804. 10.1016/j.immuni.2013.04.004.

Hettinger, J., D.M. Richards, J. Hansson, M.M. Barra, A.C. Joschko, J. Krijgsveld, and M. Feuerer. 2013. Origin of monocytes and macrophages in a committed progenitor. *Nat Immunol* 14:821-830. 10.1038/ni.2638.

Hoffman, D., Y. Tevet, S. Trzebanski, G. Rosenberg, L. Vainman, A. Solomon, S. Hen-Avivi, N.B. Ben-Moshe, and R. Avraham. 2021. A non-classical monocyte-derived macrophage subset provides a splenic replication niche for intracellular Salmonella. *Immunity* 54:2712-2723 e2716. 10.1016/j.immuni.2021.10.015.

Hu, X., A.Y. Chung, I. Wu, J. Foldi, J. Chen, J.D. Ji, T. Tateya, Y.J. Kang, J. Han, M. Gessler, R. Kageyama, and L.B. Ivashkiv. 2008. Integrated regulation of Toll-like receptor responses by Notch and interferon-gamma pathways. *Immunity* 29:691-703. 10.1016/j.immuni.2008.08.016.

Imhof, B.A., S. Jemelin, R. Ballet, C. Vesin, M. Schapira, M. Karaca, and Y. Emre. 2016. CCN1/CYR61-mediated meticulous patrolling by Ly6Clow monocytes fuels vascular inflammation. *Proc Natl Acad Sci U S A* 113:E4847-4856. 10.1073/pnas.1607710113.

Ingersoll, M.A., R. Spanbroek, C. Lottaz, E.L. Gautier, M. Frankenberger, R. Hoffmann, R. Lang, M. Haniffa, M. Collin, F. Tacke, A.J. Habenicht, L. Ziegler-Heitbrock, and G.J. Randolph. 2010. Comparison of gene expression profiles between human and mouse monocyte subsets. *Blood*

115:e10-19. 10.1182/blood-2009-07-235028.

Kang, L., X. Zhang, L. Ji, T. Kou, S.M. Smith, B. Zhao, X. Guo, I. Pineda-Torra, L. Wu, and X. Hu. 2020. The colonic macrophage transcription factor RBP-J orchestrates intestinal immunity against bacterial pathogens. *J Exp Med* 217:10.1084/jem.20190762.

Keerthivasan, S., Y. Senbabaoglu, N. Martinez-Martin, B. Husain, E. Verschueren, A. Wong, Y.A. Yang, Y. Sun, V. Pham, T. Hinkle, Y. Oei, S. Madireddi, R. Corpuz, L. Tam, S. Carlisle, M. Roose-Girma, Z. Modrusan, Z. Ye, J.T. Koerber, and S.J. Turley. 2021. Homeostatic functions of monocytes and interstitial lung macrophages are regulated via collagen domain-binding receptor LAIR1. *Immunity* 54:1511-1526 e1518. 10.1016/j.immuni.2021.06.012.

Klinakis, A., C. Lobry, O. Abdel-Wahab, P. Oh, H. Haeno, S. Buonamici, I. van De Walle, S. Cathelin, T. Trimarchi, E. Araldi, C. Liu, S. Ibrahim, M. Beran, J. Zavadil, A. Efstratiadis, T. Taghon, F. Michor, R.L. Levine, and I. Aifantis. 2011. A novel tumour-suppressor function for the Notch pathway in myeloid leukaemia. *Nature* 473:230-233. 10.1038/nature09999.

Krishnasamy, K., A. Limbourg, T. Kapanadze, J. Gamrekelashvili, C. Beger, C. Hager, V.J. Lozanovski, C.S. Falk, L.C. Napp, J. Bauersachs, M. Mack, H. Haller, C. Weber, R.H. Adams, and F.P. Limbourg. 2017. Blood vessel control of macrophage maturation promotes arteriogenesis in ischemia. *Nat Commun* 8:952. 10.1038/s41467-017-00953-2.

Landsman, L., L. Bar-On, A. Zernecke, K.W. Kim, R. Krauthgamer, E. Shagdarsuren, S.A. Lira, I.L. Weissman, C. Weber, and S. Jung. 2009. CX3CR1 is required for monocyte homeostasis and atherogenesis by promoting cell survival. *Blood* 113:963-972. 10.1182/blood-2008-07-170787.

Lewis, K.L., M.L. Caton, M. Bogunovic, M. Greter, L.T. Grajkowska, D. Ng, A. Klinakis, I.F. Charo, S. Jung, J.L. Gommerman, Ivanov, II, K. Liu, M. Merad, and B. Reizis. 2011. Notch2 receptor signaling controls functional differentiation of dendritic cells in the spleen and intestine. *Immunity* 35:780-791. 10.1016/j.immuni.2011.08.013.

Liu, K., C. Waskow, X. Liu, K. Yao, J. Hoh, and M. Nussenzweig. 2007. Origin of dendritic cells in peripheral lymphoid organs of mice. *Nat Immunol* 8:578-583. 10.1038/ni1462.

Liu, Z., Y. Gu, S. Chakarov, C. Bleriot, I. Kwok, X. Chen, A. Shin, W. Huang, R.J. Dress, C.A. Dutertre, A. Schlitzer, J. Chen, L.G. Ng, H. Wang, Z. Liu, B. Su, and F. Ginhoux. 2019. Fate Mapping via Ms4a3-Expression History Traces Monocyte-Derived Cells. *Cell* 178:1509-1525 e1519. 10.1016/j.cell.2019.08.009.

MacDonald, K.P., J.S. Palmer, S. Cronau, E. Seppanen, S. Olver, N.C. Raffelt, R. Kuns, A.R. Pettit, A. Clouston, B. Wainwright, D. Branstetter, J. Smith, R.J. Paxton, D.P. Cerretti, L. Bonham, G.R. Hill, and D.A. Hume. 2010. An antibody against the colony-stimulating factor 1 receptor depletes the resident subset of monocytes and tissue- and tumor-associated macrophages but does not inhibit inflammation. *Blood* 116:3955-3963. 10.1182/blood-2010-02-266296.

Misharin, A.V., C.M. Cuda, R. Saber, J.D. Turner, A.K. Gierut, G.K. Haines, 3rd, S. Berdnikovs, A. Filer, A.R. Clark, C.D. Buckley, G.M. Mutlu, G.R. Budinger, and H. Perlman. 2014. Nonclassical Ly6C(-) monocytes drive the development of inflammatory arthritis in mice. *Cell Rep* 9:591-604. 10.1016/j.celrep.2014.09.032.

Nahrendorf, M., F.K. Swirski, E. Aikawa, L. Stangenberg, T. Wurdinger, J.L. Figueiredo, P. Libby, R. Weissleder, and M.J. Pittet. 2007. The healing myocardium sequentially mobilizes two monocyte subsets with divergent and complementary functions. *J Exp Med* 204:3037-3047. 10.1084/jem.20070885.

Passlick, B., D. Flieger, and H.W. Ziegler-Heitbrock. 1989. Identification and characterization of a novel

monocyte subpopulation in human peripheral blood. *Blood* 74:2527-2534.

Puchner, A., V. Saferding, M. Bonelli, Y. Mikami, M. Hofmann, J.S. Brunner, M. Caldera, E. Goncalves-Alves, N.B. Binder, A. Fischer, E. Simader, C.W. Steiner, H. Leiss, S. Hayer, B. Niederreiter, T. Karonitsch, M.I. Koenders, B.K. Podesser, J.J. O'Shea, J. Menche, et al. 2018. Non-classical monocytes as mediators of tissue destruction in arthritis. *Ann Rheum Dis* 77:1490-1497. 10.1136/annrheumdis-2018-213250.

Radtke, F., H.R. MacDonald, and F. Tacchini-Cottier. 2013. Regulation of innate and adaptive immunity by Notch. *Nat Rev Immunol* 13:427-437. 10.1038/nri3445.

Sabatel, C., C. Radermecker, L. Fievez, G. Paulissen, S. Chakarov, C. Fernandes, S. Olivier, M. Toussaint, D. Pirottin, X. Xiao, P. Quatresooz, J.C. Sirard, D. Cataldo, L. Gillet, H. Bouabe, C.J. Desmet, F. Ginhoux, T. Marichal, and F. Bureau. 2017. Exposure to Bacterial CpG DNA Protects from Airway Allergic Inflammation by Expanding Regulatory Lung Interstitial Macrophages. *Immunity* 46:457-473. 10.1016/j.immuni.2017.02.016.

Sakai, M., T.D. Troutman, J.S. Seidman, Z. Ouyang, N.J. Spann, Y. Abe, K.M. Ego, C.M. Bruni, Z. Deng, J.C.M. Schlachetzki, A. Nott, H. Bennett, J. Chang, B.T. Vu, M.P. Pasillas, V.M. Link, L. Texari, S. Heinz, B.M. Thompson, J.G. McDonald, et al. 2019. Liver-Derived Signals Sequentially Reprogram Myeloid Enhancers to Initiate and Maintain Kupffer Cell Identity. *Immunity* 51:655-670 e658. 10.1016/j.immuni.2019.09.002.

Schyns, J., Q. Bai, C. Ruscitti, C. Radermecker, S. De Schepper, S. Chakarov, F. Farnir, D. Pirottin, F. Ginhoux, G. Boeckxstaens, F. Bureau, and T. Marichal. 2019. Non-classical tissue monocytes and two functionally distinct populations of interstitial macrophages populate the mouse lung. *Nat Commun* 10:3964. 10.1038/s41467-019-11843-0.

Shi, C., and E.G. Pamer. 2011. Monocyte recruitment during infection and inflammation. *Nat Rev Immunol* 11:762-774. 10.1038/nri3070.

Tacke, F., F. Ginhoux, C. Jakubzick, N. van Rooijen, M. Merad, and G.J. Randolph. 2006. Immature monocytes acquire antigens from other cells in the bone marrow and present them to T cells after maturing in the periphery. *J Exp Med* 203:583-597. 10.1084/jem.20052119.

Tamura, A., H. Hirai, A. Yokota, N. Kamio, A. Sato, T. Shoji, T. Kashiwagi, Y. Torikoshi, Y. Miura, D.G. Tenen, and T. Maekawa. 2017. C/EBPbeta is required for survival of Ly6C(-) monocytes. *Blood* 130:1809-1818. 10.1182/blood-2017-03-772962.

Thomas, G.D., R.N. Hanna, N.T. Vasudevan, A.A. Hamers, C.E. Romanoski, S. McArdle, K.D. Ross, A. Blatchley, D. Yoakum, B.A. Hamilton, Z. Mikulski, M.K. Jain, C.K. Glass, and C.C. Hedrick. 2016. Deleting an Nr4a1 Super-Enhancer Subdomain Ablates Ly6C(low) Monocytes while Preserving Macrophage Gene Function. *Immunity* 45:975-987. 10.1016/j.immuni.2016.10.011.

Urbanski, K., D. Ludew, G. Filip, M. Filip, A. Sagan, P. Szczepaniak, G. Grudzien, J. Sadowski, B. Jasiewicz-Honkisz, T. Sliwa, B. Kapelak, E. McGinnigle, T. Mikolajczyk, and T.J. Guzik. 2017. CD14(+)CD16(++) "nonclassical" monocytes are associated with endothelial dysfunction in patients with coronary artery disease. *Thromb Haemost* 117:971-980. 10.1160/TH16-08-0614.

Varol, C., L. Landsman, D.K. Fogg, L. Greenshtein, B. Gildor, R. Margalit, V. Kalchenko, F. Geissmann, and S. Jung. 2007. Monocytes give rise to mucosal, but not splenic, conventional dendritic cells. *J Exp Med* 204:171-180. 10.1084/jem.20061011.

Wang, Y.C., F. He, F. Feng, X.W. Liu, G.Y. Dong, H.Y. Qin, X.B. Hu, M.H. Zheng, L. Liang, L. Feng, Y.M. Liang, and H. Han. 2010. Notch signaling determines the M1 versus M2 polarization of macrophages in antitumor immune responses. *Cancer Res* 70:4840-4849. 10.1158/0008-

5472.CAN-10-0269.

Weber, C., K.U. Belge, P. von Hundelshausen, G. Draude, B. Steppich, M. Mack, M. Frankenberger, K.S. Weber, and H.W. Ziegler-Heitbrock. 2000. Differential chemokine receptor expression and function in human monocyte subpopulations. *J Leukoc Biol* 67:699-704. 10.1002/jlb.67.5.699.

Xu, H., J. Zhu, S. Smith, J. Foldi, B. Zhao, A.Y. Chung, H. Outtz, J. Kitajewski, C. Shi, S. Weber, P. Saftig, Y. Li, K. Ozato, C.P. Blobel, L.B. Ivashkiv, and X. Hu. 2012. Notch-RBP-J signaling regulates the transcription factor IRF8 to promote inflammatory macrophage polarization. *Nat Immunol* 13:642-650. 10.1038/ni.2304.

Yona, S., K.W. Kim, Y. Wolf, A. Mildner, D. Varol, M. Breker, D. Strauss-Ayali, S. Viukov, M. Guilliams, A. Misharin, D.A. Hume, H. Perlman, B. Malissen, E. Zelzer, and S. Jung. 2013. Fate mapping reveals origins and dynamics of monocytes and tissue macrophages under homeostasis. *Immunity* 38:79-91. 10.1016/j.immuni.2012.12.001.

Zhao, B., S.N. Grimes, S. Li, X. Hu, and L.B. Ivashkiv. 2012. TNF-induced osteoclastogenesis and inflammatory bone resorption are inhibited by transcription factor RBP-J. *J Exp Med* 209:319-334. 10.1084/jem.20111566.

**Acknowledgements:**

We thank the core facility at Institute for Immunology, Tsinghua University for valuable technical assistance.

**Funding:**

This research was supported by National Natural Science Foundation of China grants (31821003, 31991174, 32030037 and 82150105 to X. Hu), a Ministry of Science and Technology of China grant (2020YFA0509100 to X. Hu), and funds from Tsinghua-Peking Center for Life Sciences and Institute for Immunology at Tsinghua University (to X. Hu).

**Author contributions:**

T. Kou designed and performed experiments, analyzed and interpreted data, and wrote the manuscript. L. Kang designed and performed experiments, analyzed and interpreted data. B. Zhang provided advice on RNA-seq analyses. J. Li performed experiments. B. Zhao provided advice on experiments. W. Zeng provided advice on experiments. X. Hu conceptualized the project, supervised experiments, interpreted data, and wrote the manuscript.

**Declaration of interests:**

The authors declare no competing interests.

**Data availability:**

Sequencing data sets are deposited in the Genome Expression Omnibus with assigned accession numbers as follows: RNA-seq (GEO accession no. GSE208772).

**Materials and methods**

**Mice**

*Cx3cr1*$^{gfp/gfp}$ mice (JAX stock 005582; Jung et al., 2000) and *Ccr2*$^{RFP/RFP}$ mice (JAX stock 017586) were purchased from the Jackson Laboratory. Mice with a myeloid-

specific deletion of the *Rbpj* were generated by crossing *Rbpj*$^{fl/fl}$ mice to *Lyz2*-Cre mice as described previously (Hu et al., 2008). *Rbpj*$^{fl/fl}$*Lyz2*$^{cre/cre}$ were crossed to *Cx3cr1*$^{gfp/gfp}$ mice to obtain *Lyz2*$^{cre/cre}$*Cx3cr1*$^{gfp/+}$and *Rbpj*$^{fl/fl}$*Lyz2*$^{cre/cre}$*Cx3cr1*$^{gfp/+}$ mice. C*x3cr1*$^{gfp/+}$ mice were obtained by crossing *Cx3cr1*$^{gfp/gfp}$ with C57/BL6 CD45.1$^{+}$ mice. *Rbpj*$^{fl/fl}$*Lyz2*$^{cre/cre}$ mice were crossed with *Ccr2*$^{RFP/RFP}$ mice to obtain *Lyz2*$^{cre/cre}$*Ccr2*$^{RFP/+}$, *Lyz2*$^{cre/cre}$*Ccr2*$^{RFP/RFP}$, *Rbpj*$^{fl/fl}$*Lyz2*$^{cre/cre}$*Ccr2*$^{RFP/+}$ and *Rbpj*$^{fl/fl}$*Lyz2*$^{cre/cre}$*Ccr2*$^{RFP/RFP}$ mice. All mice were maintained under specific pathogen-free conditions. All animal experimental protocols were approved by the Institutional Animal Care and Use Committees of Tsinghua University. Gender- and age-matched mice were used at 7–12 weeks old for experiments.

**Quantitative RT-PCR**

Blood monocytes were sorted by flow cytometry. The total RNA was extracted using total RNA purification kit (GeneMarkbio) and reversely transcribed to cDNA by M-MLV Reverse Transcriptase (Takara). qPCR was performed on a real-time PCR system (StepOnePlus; Applied Biosystems) using FastSYBR mixture (CWBIO). *Gapdh* messenger RNA was used as internal control to normalize the expression of target genes. Primer sequences are provided in supplemental Table 1.

**Table 1: Primers sequences for regular qPCR used in this study**

| Gene | Forward primer | Reverse primer |
|---|---|---|
| *Gapdh* | ATCAAGAAGGTGGTGAAGCA | AGACAACCTGGTCCTCAGTGT |
| *Rbpj* | ACCCCTGTGCCTGTCGTAGA A | TCCCGGAATGCAGAAATGTC |
| *Nr4a1* | TTGAGCTTGAATACAGGGCA | AGTTGGGGGAGTGTGCTAGA |
| *Ccr2* | CCTTGGGAATGAGTAACTGT GTGAT | ATGGAGAGATACCTTCGGAAC TTCT |

**RNA-seq analysis**

Ly6C$^{hi}$ and Ly6C$^{lo}$ blood monocytes were isolated from *Rbpj*$^{+/+}$*Lyz2*$^{cre/cre}$ and *Rbpj*$^{fl/fl}$*Lyz2*$^{cre/cre}$ mice, and total RNA was extracted using total RNA purification kit (GeneMarkbio). RNA was converted into RNA-seq libraries, which were sequenced

with the pair-end option using an Illumina-HiSeq2500 platform at Beijing Genomics Institute (BGI), China. The significantly down-regulated genes were identified with P value <0.05 and (FPKM + 1) fold changes ≤0.2, and significantly up-regulated genes were identified with P value <0.05 and (FPKM + 1) fold changes ≥5.7. The RNA-seq data are deposited in Gene Expression Omnibus under accession number GSE208772

**Annexin V staining**

Annexin V and 7-amino-actinomycin D (7-AAD) were used for identification of apoptotic monocytes by flow cytometry. Blood cells were stained with annexin V (eBioscience) and 7-AAD (Biolegend) according to the manufacturers' protocols.

**EdU pulsing and latex beads labeling**

Mice were injected intravenously with a single 1 mg EdU (Thermo Scientific). BM and blood cells were collected and stained with Fluorescence-conjugated mAb against CD45, CD11b, Ly6G, CD115 and Ly6C. Cells were then fixed, permeabilized and stained with reaction cocktail using EdU Assay Kit. Labeled cells were analyzed by flow cytometry.

Mice were injected intravenously with a single 10 μl latex beads (Polysciences) in 250 μl PBS. Blood cells were harvested at indicated time. Cells were then stained for CD45, CD11b, Ly6G, CD115, Ly6C, and analyzed by flow cytometry.

**In vivo labeling of sinusoidal leukocytes**

Mice were injected intravenously with 1 μg of PE-conjugated anti-CD45 antibodies. Two minutes after antibody injection, mice were sacrificed, and bone marrow were harvested. BM cells were then stained and analyzed by flow cytometry.

**Generation of BM chimera**

C57/BL6 CD45.2$^{+}$ mice were lethally irradiated in two doses of 5.5Gy 2 h apart. 0.8 × $10^{5}$ BM cells from *Rbpj*$^{+/+}$*Lyz2*$^{cre/cre}$ mice (CD45.2$^{+}$) or *Rbpj*$^{fl/fl}$*Lyz2*$^{cre/cre}$ mice (CD45.2$^{+}$) were mixed with 3.2× $10^{5}$ BM cells from *Cx3cr1*$^{gfp/+}$ mice (CD45.1$^{+}$), and injected

intravenously into recipient mice. Mice were used for experiments 8 weeks after irradiation.

655

**Adoptive transfers**

BM GFP$^{+}$Ly6C$^{hi}$ monocytes were sorted from *Lyz2*$^{cre/cre}$*Cx3cr1*$^{gfp/+}$ or *Rbpj*$^{fl/fl}$*Lyz2*$^{cre/cre}$*Cx3cr1*$^{gfp/+}$ mice, and transferred to *Ccr2*$^{RFP/RFP}$ mice. Blood cells were collected 60 hours later for flow cytometry analyses.

660

**Parabiosis**

*Cx3cr1*$^{gfp/+}$ CD45.1$^{+}$ mice were surgically joined with age-matched female *Rbpj*$^{fl/fl}$*Lyz2*$^{cre/cre}$ or *Rbpj*$^{+/+}$*Lyz2*$^{cre/cre}$ CD45.2$^{+}$ mice at the age of 6 weeks. Bloods were obtained via cardiac puncture, and cell populations were analyzed by flow cytometry at

665 4 weeks after the surgery.

**Intranasal instillations of LPS**

*Rbpj*$^{+/+}$*Lyz2*$^{cre/cre}$ or *Rbpj*$^{fl/fl}$*Lyz2*$^{cre/cre}$ mice were anesthetized with isoflurane and intranasally instilled with 10 μg LPS in 25 μl of PBS. Lungs were harvested 4 days later

670 for flow cytometry analyses.

**Immunofluorescence histology**

Lungs from *Rbpj*$^{fl/fl}$*Lyz2*$^{cre/cre}$*Cx3cr1*$^{gfp/+}$ and *Lyz2*$^{cre/cre}$*Cx3cr1*$^{gfp/+}$ mice were fixed in 1% paraformaldehyde and incubated in 30% sucrose separately overnight at 4°C. The

675 samples were then incubated in the mixture of 30% sucrose and OTC compound (Sakura Finetek) overnight at 4°C. The tissues were embedded and frozen in OCT compound and then cut at 10-μm thickness. Tissue sections were dried for 10 min at 50°C and then fixed in 1% paraformaldehyde at room temperature for 10 min, permeabilized in PBS/0.5% Triton X-100/0.3 M glycine for 10 min and blocked in

680 PBS/5% goat serum for 1 h at room temperature. Sections were stained with rabbit anti-mouse GFP antibodies (1:1000; EASYBIO) overnight at 4°C, and washed with PBS/0.1% Tween-20 for 30 min three times at room temperature. Sections were then incubated

with AF488-conjugated goat anti-rabbit antibodies (1:200; proteintech) for 2 h at room temperature, and washed with PBS/0.1% Tween-20 for 30 min three times at room temperature. Sections were stained with DAPI (Solarbio) for 7 min, washed in PBS for 8 min two times at room temperature and mounted with SlowFade Diamond Antifade Mountant (Life Technologies).

**Cell isolation and flow cytometry**

Peripheral blood (PB) was sampled by eyeball extirpating, spleens were mashed through a 70-μm strainer, and bone marrow cells were collected from femurs. Lungs were perfused with 5 ml of HBSS (MACGENE) through the right ventricle, excised, and digested in HBSS containing 5% FBS, 1 mg/ml collagenase type I (Sigma-Aldrich) and 0.05 mg/ml DNase I (Sigma-Aldrich) for 1 h at 37 °C. The digested tissues were homogenized by shaking, passed through a 70-μm cell strainer to create a single cell suspension. The suspension was enriched in mononuclear cells and harvested from the 1.080:1.038 g $ml^{-1}$ interface using a density gradient (Percoll from GE Healthcare). BM, Spleen, PB and lung cells were stained with fluorescently conjugated antibodies. The absolute number of cells was counted by using CountBright™ Absolute Counting Beads (Invitrogen).

Antibodies against CD45 (30-F11), Ly6C (HK1.4), CD64 (X54-5/7.1), CD206 (C068C2), CD16.2 (9E9), CD45.1 (A20), F4/80 (BM8), Biotin, CCR2 (SA203G11) and CD3ε (145-2C11) were purchased from BioLegend. Antibodies against Ly6G (1A8-Ly6g), CD11b (M1/70), CD115(AFS98), CD117(2B8), CD135 (A2F10), CD11c (N418), CD206 (MR6F3), CD45.2 (104), Nur77 (12.14), Ki-67 (SolA15) and lineage maker were purchased from eBioscience. Fluorescence-conjugated mAb against Ly6C (AL-21) were purchased from BD Biosciences. Isotype-matched antibodies (eBioscience) were used for control staining. All antibodies were used in 1:400 dilutions, and surface antigens were stained on ice for 30 min.

For intracellular staining, cells were stained with antibodies to surface antigens, fixed

and permeabilized with the Cytofix/Cytoperm Fixation/Permeabilization Solution Kit (BD Biosciences), and stained with antibodies or isotype control diluted in permeabilization buffer separately for 30 min at room temperature.

Cells were analyzed on FACSFortessa or FACSAria III flow cytometer (BD Biosciences) using FlowJo software.

**Statistical analysis**

Statistical analysis was performed using GraphPad Prism software. All results are shown as mean ± SEM. Statistical significance was determined using Student's unpaired t test. Statistical significance was defined as $P < 0.05$.

**Figure Legends:**

**Figure 1. RBP-J deficient mice display more Ly6C$^{lo}$ blood monocytes.**

745 (A) Blood Ly6C$^{hi}$ and Ly6C$^{lo}$ monocytes in *Rbpj*$^{+/+}$*Lyz2*$^{cre/cre}$ control and *Rbpj*$^{fl/fl}$*Lyz2*$^{cre/cre}$ mice were determined by flow cytometry analyses (FACS). Representative FACS plots (left) and cumulative data of cell ratio (right) are shown.

(B and C) Representative FACS plots and cumulative data quantitating percentages of BM monocyte subsets (B) and myeloid progenitor cells (C) (CD45$^{+}$CD11b$^{+}$Ly6G$^{-}$

750 CD115$^{+}$ Ly6C$^{hi}$ monocyte; CD45$^{+}$CD11b$^{+}$Ly6G$^{-}$CD115$^{+}$Ly6C$^{lo}$ monocyte; MDP, CD45$^{+}$Lin$^{-}$CD117$^{+}$CD115$^{+}$CD135$^{+}$ Ly6C$^{-}$; cMoP, CD45$^{+}$Lin$^{-}$CD11b$^{-}$CD117$^{+}$CD115$^{+}$ CD135$^{-}$Ly6C$^{+}$). Lin: CD3, B220, Ter119, and Gr-1, CD11b.

(D) Experimental outline for panel (E).

(E) Cumulative data quantitating percentages of sinusoidal monocytes (CD45$^{+}$) within

755 total BM Ly6C$^{lo}$ monocytes.

Data are pooled from at least 2 independent experiments; n ≥ 4 in each group. Data are shown as mean ± SEM; n.s., not significant; **, P < 0.01 (two-tailed Student's unpaired t test). Each symbol represents an individual mouse.

760 **Figure 2. Monocyte subsets in RBP-J deficient mice display normal cell death.**

(A) Representative FACS plots of monocyte subsets in blood stained with 7-AAD and Annexin V.

(B) FACS analysis of Ki-67 expression in *Rbpj*$^{+/+}$*Lyz2*$^{cre/cre}$ control and *Rbpj*$^{fl/fl}$*Lyz2*$^{cre/cre}$ blood monocyte subsets. Black lines represent control mice and red lines represent

765 RBP-J deficient mice.

(C) Analysis of time course of EdU incorporation of monocyte subsets in BM and blood after a single 1 mg EdU pulsing. The percentages of EdU$^{+}$ cells among the indicated monocyte subsets are shown.

(D) Experimental outline for panel (E).

770 (E) Analysis of time course of latex beads incorporation of monocyte subsets in blood after latex beads injection. The percentages of latex$^{+}$ cells among the indicated monocyte subsets are shown.

(F) Cartoon depicting the adoptive transfer. BM GFP$^{+}$Ly6C$^{hi}$ monocytes were sorted from *Lyz2*$^{cre/cre}$*Cx3cr1*$^{gfp/+}$ or *Rbpj*$^{fl/fl}$*Lyz2*$^{cre/cre}$*Cx3cr1*$^{gfp/+}$ mice and transferred into
775 *Ccr2*$^{RFP/RFP}$ recipient mice. Sixty hours after transfer, cell fate was analyzed.

(G) Representative FACS plots are shown in the left panel, and the frequencies of GFP$^{+}$Ly6C$^{lo}$ monocytes within total Ly6C$^{lo}$ monocytes are shown in the right panel.

Data are pooled from 2 independent experiments (G); n ≥ 2 in each group (C, E and G). Data are shown as mean ± SEM; n.s., not significant; (two-tailed Student's unpaired t
780 test). Each symbol represents an individual mouse (E and G).

**Figure 3. The role of RBP-J in blood Ly6C$^{lo}$ monocytes is cell intrinsic.**

(A) Cartoon depicting the bone marrow transplantation. BM recipient 6-week-old male C57BL/6 mice (CD45.2) were lethally irradiated. BM cells from donor mice
785 (*Rbpj*$^{+/+}$*Lyz2*$^{cre/cre}$ or *Rbpj*$^{fl/fl}$*Lyz2*$^{cre/cre}$ and CD45.1, *Cx3cr1*$^{gfp/+}$) were collected and transferred into recipient mice. Mice were used after 8 weeks of bone marrow reconstitution.

(B) Representative FACS plots (left) and cumulative data (right) quantitating the frequency of *Rbpj*$^{+/+}$*Lyz2*$^{cre/cre}$ and *Rbpj*$^{fl/fl}$*Lyz2*$^{cre/cre}$ donor cells among Ly6C$^{hi}$ and
790 Ly6C$^{lo}$ monocytes in the blood of recipient mice.

(C) Cartoon depicting the generation of *Rbpj*$^{+/+}$*Lyz2*$^{cre/cre}$ control or *Rbpj*$^{fl/fl}$*Lyz2*$^{cre/cre}$ and *Cx3cr1*$^{gfp/+}$ parabiotic pairs.

(D) Representative FACS plots (left) and cumulative data (right) quantitating percentages of monocyte subsets derived from control or RBP-J deficient mice in
795 control or RBP-J deficient mice.

(E) Representative FACS plots (left) and cumulative data (right) quantitating percentages of monocyte subsets derived from control or RBP-J deficient mice in *Cx3cr1*$^{gfp/+}$ mice.

Data are pooled from at least 2 independent experiments; n ≥ 6 in each group. Data are
800 shown as mean ± SEM; n.s., not significant; ***, P < 0.001; ****, P < 0.0001 (two-tailed Student's unpaired t test). Each symbol represents an individual mouse. SSC-A, side scatter area.

**Figure 4. Phenotypic markers in Ly6C$^{lo}$ monocytes are changed in RBP-J deficient mice.**

805 (A) Heatmap of RNA-seq dataset showing the top 20 downregulated and upregulated genes in blood Ly6C$^{lo}$ monocytes from *Rbpj*$^{fl/fl}$*Lyz2*$^{cre/cre}$ versus *Rbpj*$^{+/+}$*Lyz2*$^{cre/cre}$ control mice. Blue and red font indicates downregulated and upregulated genes in RBP-J deficient Ly6C$^{lo}$ monocytes respectively.

(B) Representative FACS plots, cumulative MFI, and qPCR analysis of CCR2/CD11c

810 expression in control and RBP-J deficient blood monocyte subsets. Shaded curves represent isotype control, black lines represent control mice and red lines represent RBP-J deficient mice.

(C) PCA of indicated cell types.

(D) Representative FACS plots and cumulative MFI of CCR2/CD11c expression in

815 blood monocyte subsets derived from control or RBP-J deficient mice. Black lines represent control mice, and red lines represent RBP-J deficient mice.

Data are pooled from 2 independent experiments (B and D); n ≥ 6 in each group. Data are shown as mean ± SEM; n.s., not significant; **, P < 0.01; ****, P < 0.0001 (two-tailed Student's unpaired t test). Each symbol represents an individual mouse.

820

**Figure 5. Blood Ly6C$^{lo}$ monocytes are decreased in DKO mice.**

(A) Representative FACS plots and cumulative MFI of CCR2 expression in *Lyz2*$^{cre/cre}$*Ccr2*$^{RFP/+}$ control, *Rbpj*$^{fl/fl}$*Lyz2*$^{cre/cre}$*Ccr2*$^{RFP/+}$ and *Rbpj*$^{fl/fl}$*Lyz2*$^{cre/cre}$*Ccr2*$^{RFP/RFP}$ (DKO) blood Ly6C$^{hi}$ and Ly6C$^{lo}$ monocytes are shown.

825 (B and C) Blood monocyte subsets in control, RBP-J deficient and DKO mice were determined by FACS. Representative FACS plots (B) and cumulative data of cell ratio (C) are shown.

(D) Representative FACS plots and cumulative MFI of CD11c expression in control, RBP-J deficient and DKO blood Ly6C$^{hi}$ and Ly6C$^{lo}$ monocytes are shown.

830 Data are pooled from at least 2 independent experiments; n ≥ 5 in each group. Data are shown as mean ± SEM; n.s., not significant; **, P < 0.01; ***, P < 0.001; ****, P < 0.0001 (two-tailed Student's unpaired t test). Each symbol represents an individual

mouse.

835 **Figure 6. RBP-J deficient mice exhibit more lung Ly6C$^{lo}$ monocytes and CD16.2$^{+}$ IM.**

(A and B) Indicated populations in the lungs of *Rbpj*$^{+/+}$*Lyz2*$^{cre/cre}$ and *Rbpj*$^{fl/fl}$*Lyz2*$^{cre/cre}$ mice were determined by FACS. Representative FACS plots (A) and cumulative data of cell ratio and absolute numbers (B) are shown.

840 (C) Immunofluorescence staining for GFP$^{+}$ cells in the lungs from *Lyz2*$^{cre/cre}$*Cx3cr1*$^{gfp/+}$ and *Rbpj*$^{fl/fl}$*Lyz2*$^{cre/cre}$*Cx3cr1*$^{gfp/+}$ mice (CX3CR1 [green]; DAPI [blue]). Scale bars represent 50 μm.

(D and E) *Rbpj*$^{+/+}$*Lyz2*$^{cre/cre}$ and *Rbpj*$^{fl/fl}$*Lyz2*$^{cre/cre}$ mice were instilled intranasally with PBS or PBS containing LPS, and lungs were harvested at the indicated time points.

845 Representative FACS plots (D) and cumulative data of cell ratio and absolute numbers (E) are shown.

Data are pooled from at least 2 independent experiments; n ≥ 4 in each group. Data are shown as mean ± SEM; n.s., not significant; *, P < 0.05; **, P < 0.01; ****, P < 0.0001 (two-tailed Student's unpaired t test). Each symbol represents an individual mouse.

850

**Figure 7. DKO mice lack lung Ly6C$^{lo}$ monocytes and CD16.2$^{+}$ IM.**

(A) Representative FACS plots of lung monocyte and IM subsets in *Lyz2*$^{cre/cre}$*Ccr2*$^{RFP/+}$, *Rbpj*$^{fl/fl}$*Lyz2*$^{cre/cre}$*Ccr2*$^{RFP/+}$, *Lyz2*$^{cre/cre}$*Ccr2*$^{RFP/RFP}$ and *Rbpj*$^{fl/fl}$*Lyz2*$^{cre/cre}$*Ccr2*$^{RFP/RFP}$ mice.

(B and C) Cumulative data of cell ratio and absolute numbers of monocyte (B) and IM

855 (C) subsets.

Data are pooled from 2 independent experiments; n ≥ 4 in each group. Data are shown as mean ± SEM; n.s., not significant; *, P < 0.05; **, P < 0.01; ***, P < 0.001; ****, P < 0.0001 (two-tailed Student's unpaired t test). Each symbol represents an individual mouse.

860

**Figure 1 - Figure supplement 1. Control and RBP-J deficient mice show similar neutrophils.**

(A) qPCR analysis of *Rbpj* expression in sorted monocyte subsets from control and RBP-J deficient mice.

865 (B) Blood and BM $CD45^{+}CD11b^{+}Ly6G^{+}$ neutrophils were determined by FACS. Cumulative data of cell ratio are shown.

(C) Spleen monocyte subsets were determined by FACS. Representative FACS plots (left) and cumulative data of cell ratio and absolute numbers (right) are shown.

Data are pooled from at least 2 independent experiments; $n \geq 2$ in each group. Data are

870 shown as mean ± SEM; n.s., not significant; *, $P < 0.05$ (two-tailed Student's unpaired t test). Each symbol represents an individual mouse.

**Figure 2 - Figure supplement 1. The conversion of $Ly6C^{hi}$ monocyte is identical in control and RBP-J deficient mice.**

875 (A) Representative FACS plots, cumulative MFI and qPCR analysis of Nr4a1 expression in control and RBP-J deficient blood monocyte subsets. Shaded curves represent isotype control, black lines represent control mice, and red lines represent RBP-J deficient mice.

(B) Representative FACS plots of $GFP^{+}Ly6C^{hi}$ monocytes in recipient.

880 Data are pooled from 2 independent experiments (A); $n \geq 4$ in each group. Data are shown as mean ± SEM; n.s., not significant (two-tailed Student's unpaired t test). Each symbol represents an individual mouse.

**Figure 3 - Figure supplement 1. Cell-intrinsic requirement of RBP-J for $Ly6C^{lo}$**

885 **maintenance.**

(A) Representative FACS plots (left) and cumulative data (right) quantitating percentages of blood neutrophils in recipient mice.

(B) BM neutrophils and $Ly6C^{hi}$ monocytes in recipient mice were determined by FACS.

(C) $CD4^{+}$ T cells and $CD19^{+}$ B cells were analyzed by FACS in parabiotic mice.

890 Data are pooled from at least 2 independent experiments (A and C); $n \geq 4$ in each group. Data are shown as mean ± SEM; n.s., not significant (two-tailed Student's unpaired t test). Each symbol represents an individual mouse.

**Figure 4 - Figure supplement 1. Normal expression of CCR2 and CD11c in BM monocytes.**

895 (A) Cumulative MFI of CCR2 expression in BM monocyte subsets.

(B) FACS plots of CCR2 and CD11c in BM Ly6C$^{hi}$ and Ly6C$^{lo}$ monocytes from control and RBP-J deficient mice.

Data are pooled from 3 independent experiments (A); n ≥ 7 in each group. Data are shown as mean ± SEM; n.s., not significant (two-tailed Student's unpaired t test). Each

900 symbol represents an individual mouse.

**Figure 6 - Figure supplement 1. RBP-J is not required for turnover of lung Ly6C$^{lo}$ monocytes and CD16.2$^{+}$ IM.**

(A and B) Incorporation of EdU was assessed 24 hours after injection. BM monocyte

905 subsets were used as controls. FACS plots (A) and representative data (B) are shown. Each symbol represents an individual mouse.

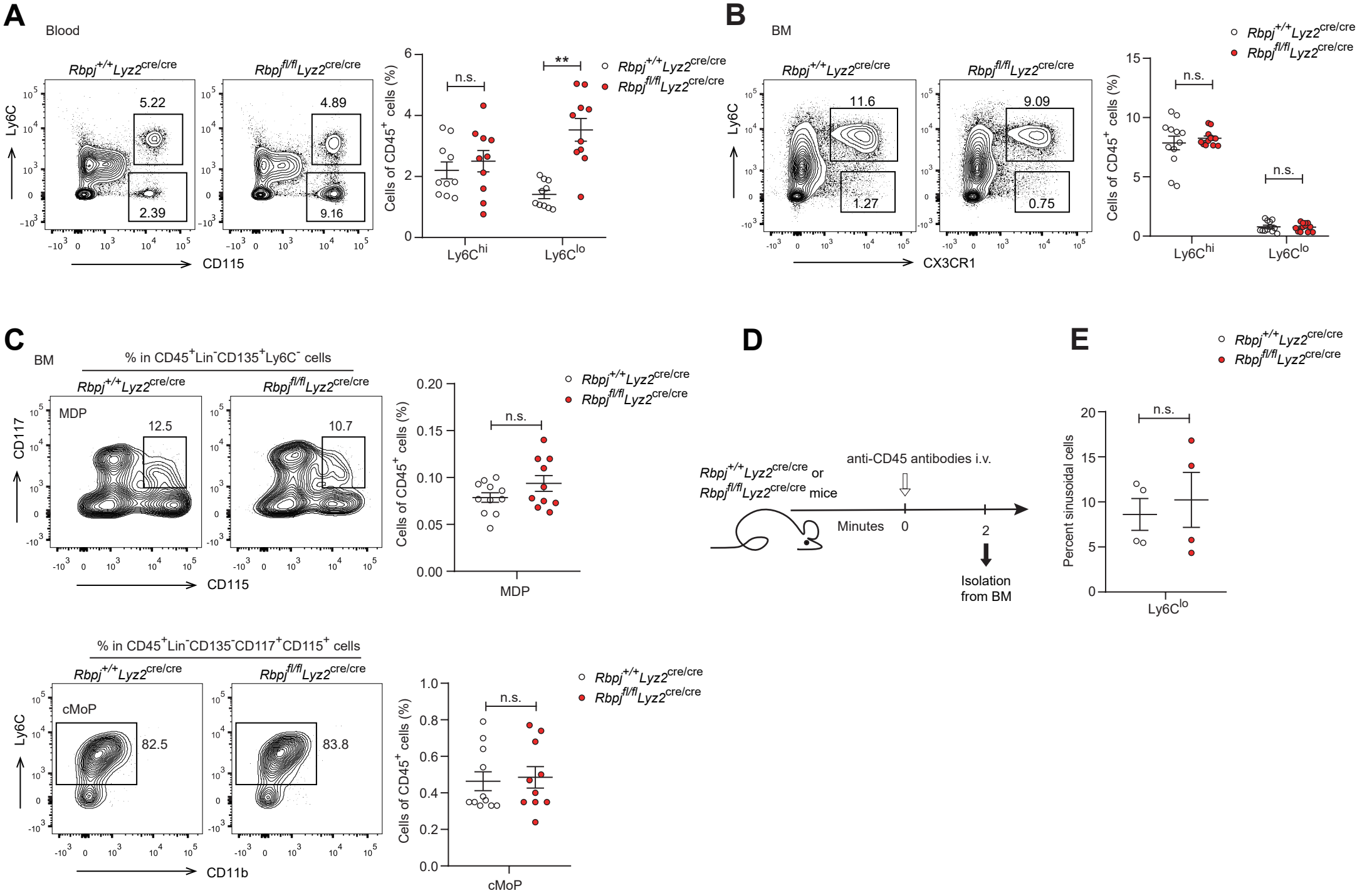
A
Blood
Rbpj+/+Lyz2cre/cre
Rbpjfl/flLyz2cre/cre
5.22
2.39
4.89
9.16
Ly6C
CD115
Cells of CD45+ cells (%)
n.s.
**
Ly6Chi
Ly6Clo
B
BM
11.6
1.27
9.09
0.75
CX3CR1
C
% in CD45+Lin-CD135+Ly6C- cells
MDP
12.5
10.7
CD117
CD115
% in CD45+Lin-CD135-CD117+CD115+ cells
cMoP
82.5
83.8
CD11b
D
anti-CD45 antibodies i.v.
Rbpj+/+Lyz2cre/cre or
Rbpjfl/flLyz2cre/cre mice
Minutes
0
2
Isolation
from BM
E
Percent sinusoidal cells

Figure 1

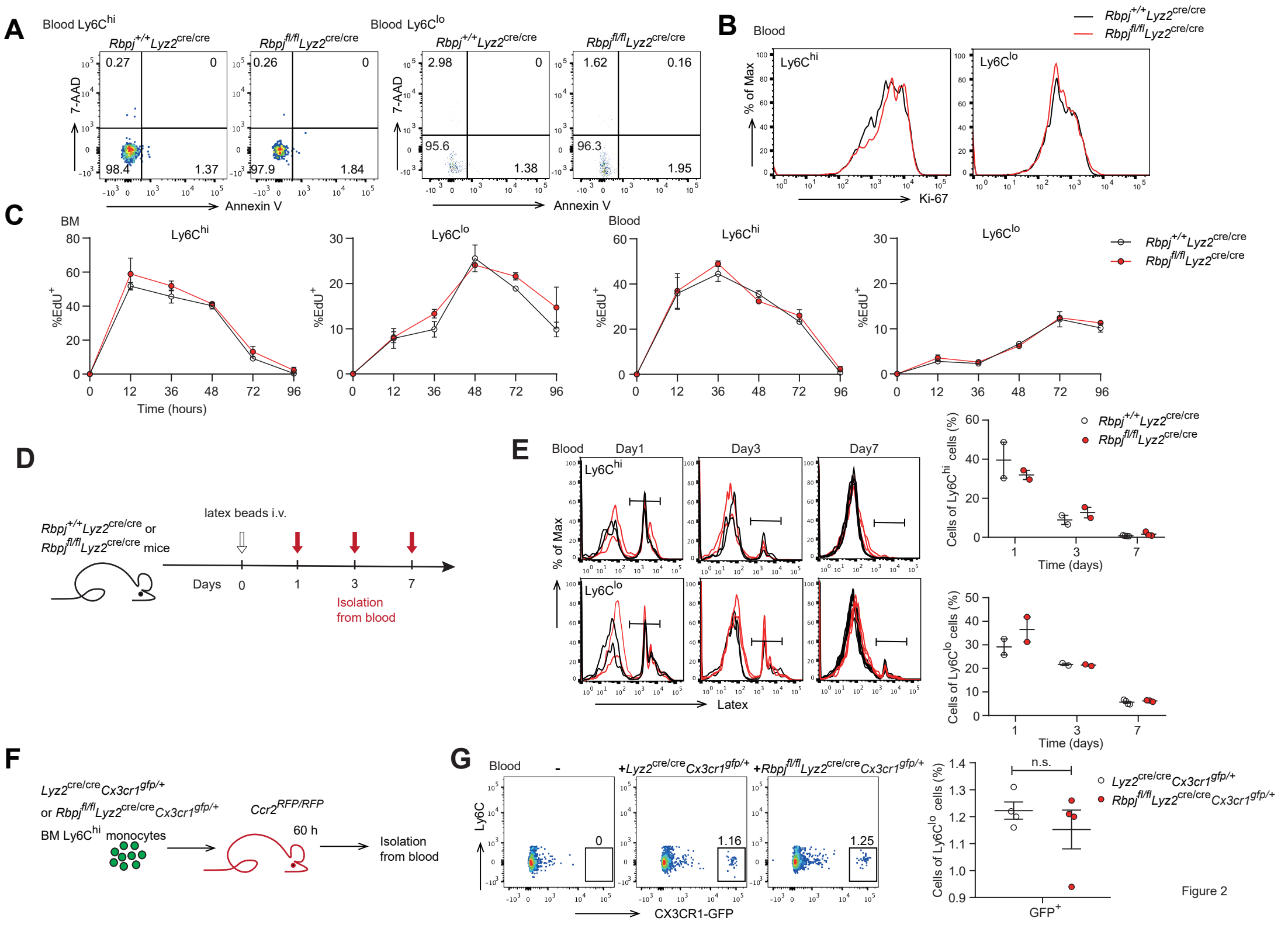
A
Blood Ly6C^hi
Rbpj+/+Lyz2cre/cre
Rbpjfl/flLyz2cre/cre
Blood Ly6C^lo
7-AAD
Annexin V
0.27
0
98.4
1.37
0.26
0
97.9
1.84
2.98
0
95.6
1.38
1.62
0.16
96.3
1.95
B
Blood
Ly6C^hi
Ly6C^lo
% of Max
Ki-67
C
BM
Blood
%EdU+
Time (hours)
D
Rbpj+/+Lyz2cre/cre or
Rbpjfl/flLyz2cre/cre mice
latex beads i.v.
Days 0 1 3 7
Isolation
from blood
E
Blood Day1 Day3 Day7
Latex
Cells of Ly6C^hi cells (%)
Cells of Ly6C^lo cells (%)
Time (days)
F
Lyz2cre/creCx3cr1gfp/+
or Rbpjfl/flLyz2cre/creCx3cr1gfp/+
BM Ly6C^hi monocytes
Ccr2RFP/RFP
60 h
Isolation
from blood
G
Blood
-
+Lyz2cre/creCx3cr1gfp/+
+Rbpjfl/flLyz2cre/creCx3cr1gfp/+
Ly6C
CX3CR1-GFP
n.s.
GFP+
Figure 2

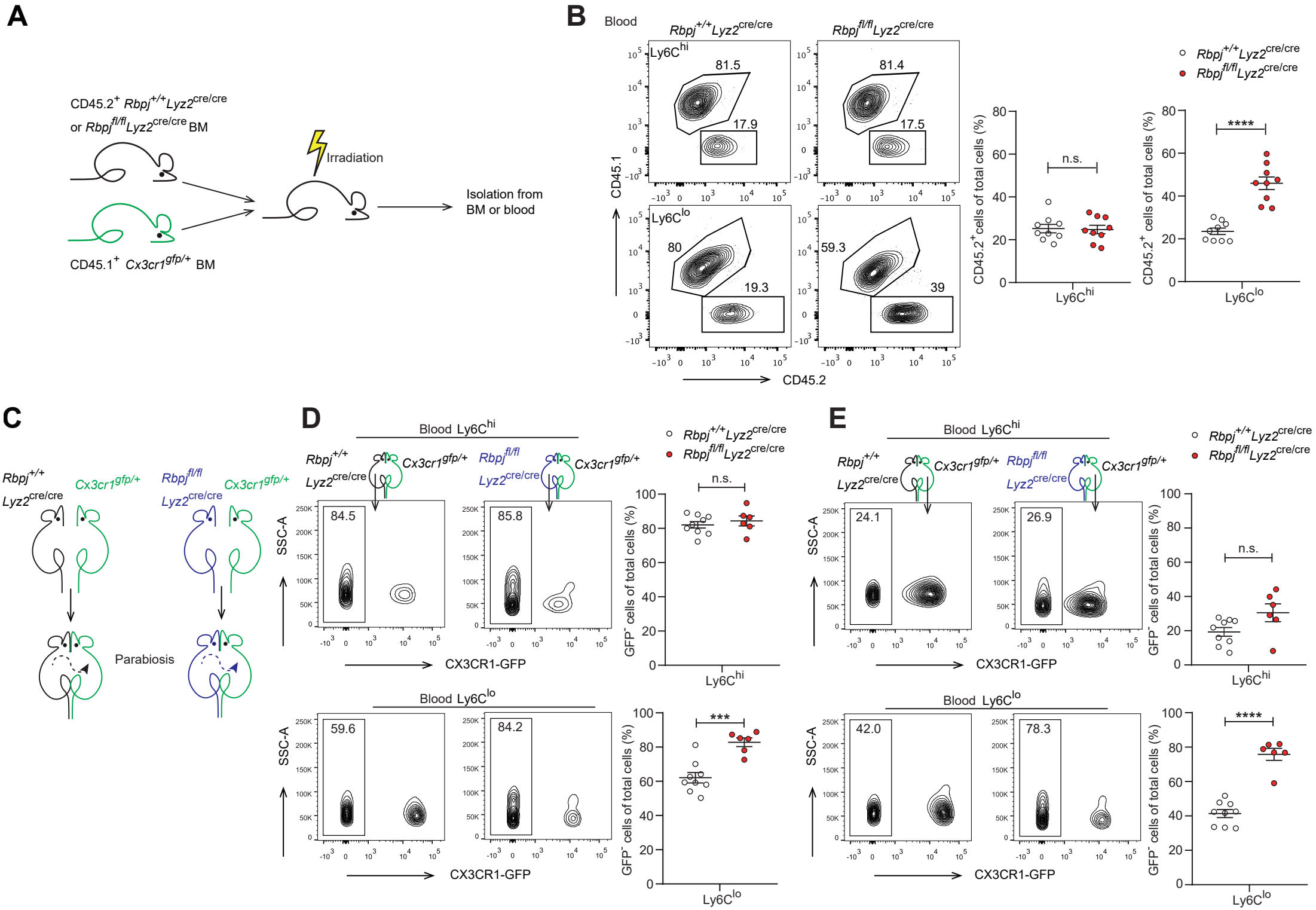
A
CD45.2+ Rbpj+/+Lyz2cre/cre
or Rbpjfl/flLyz2cre/cre BM
Irradiation
Isolation from
BM or blood
CD45.1+ Cx3cr1gfp/+ BM
B
Blood
Rbpj+/+Lyz2cre/cre
Rbpjfl/flLyz2cre/cre
Ly6Chi
81.5
17.9
81.4
17.5
Ly6Clo
80
19.3
59.3
39
CD45.1
CD45.2
n.s.
****
CD45.2+ cells of total cells (%)
Ly6Chi
Ly6Clo
C
Rbpj+/+
Lyz2cre/cre
Cx3cr1gfp/+
Rbpjfl/fl
Lyz2cre/cre
Cx3cr1gfp/+
Parabiosis
D
Blood Ly6Chi
84.5
85.8
SSC-A
CX3CR1-GFP
n.s.
GFP- cells of total cells (%)
Blood Ly6Clo
59.6
84.2
***
E
Blood Ly6Chi
24.1
26.9
n.s.
Blood Ly6Clo
42.0
78.3
****

Figure 3

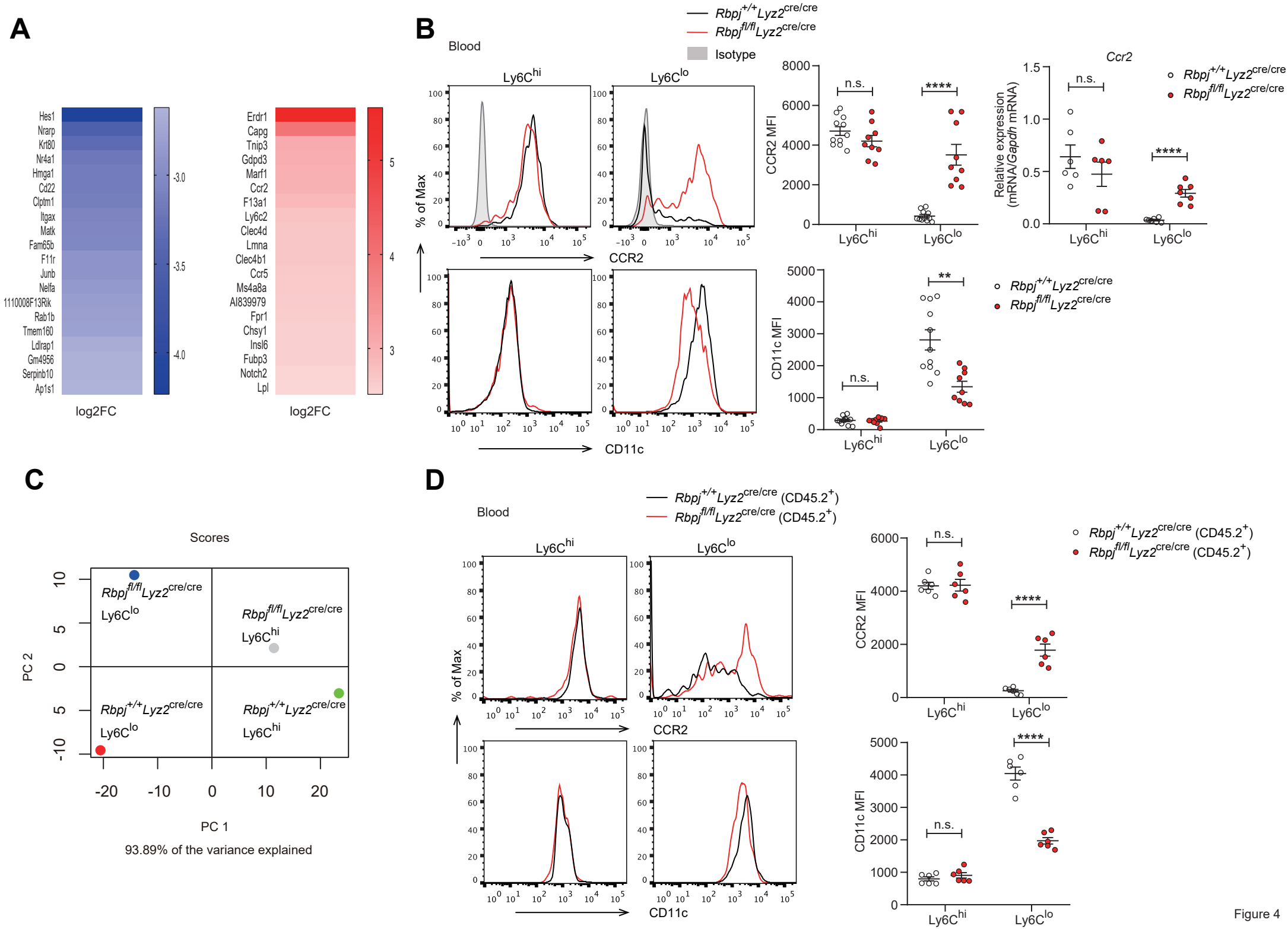
A
Hes1
Nrarp
Krt80
Nr4a1
Hmga1
Cd22
Clptm1
Itgax
Matk
Fam65b
F11r
Junb
Nelfa
1110008F13Rik
Rab1b
Tmem160
Ldlrap1
Gm4956
Serpinb10
Ap1s1
-3.0
-3.5
-4.0
log2FC
Erdr1
Capg
Tnip3
Gdpd3
Marf1
Ccr2
F13a1
Ly6c2
Clec4d
Lmna
Clec4b1
Ccr5
Ms4a8a
AI839979
Fpr1
Chsy1
Insl6
Fubp3
Notch2
Lpl
5
4
3
log2FC
B
Blood
Rbpj+/+Lyz2cre/cre
Rbpjfl/flLyz2cre/cre
Isotype
Ly6Chi
Ly6Clo
% of Max
CCR2
CD11c
CCR2 MFI
CD11c MFI
n.s.
****
**
Ccr2
Relative expression (mRNA/Gapdh mRNA)
C
Scores
Rbpjfl/flLyz2cre/cre Ly6Clo
Rbpjfl/flLyz2cre/cre Ly6Chi
Rbpj+/+Lyz2cre/cre Ly6Clo
Rbpj+/+Lyz2cre/cre Ly6Chi
PC 2
PC 1
93.89% of the variance explained
D
Blood
Rbpj+/+Lyz2cre/cre (CD45.2+)
Rbpjfl/flLyz2cre/cre (CD45.2+)
Ly6Chi
Ly6Clo
% of Max
CCR2
CD11c
CCR2 MFI
CD11c MFI
n.s.
****

Figure 4

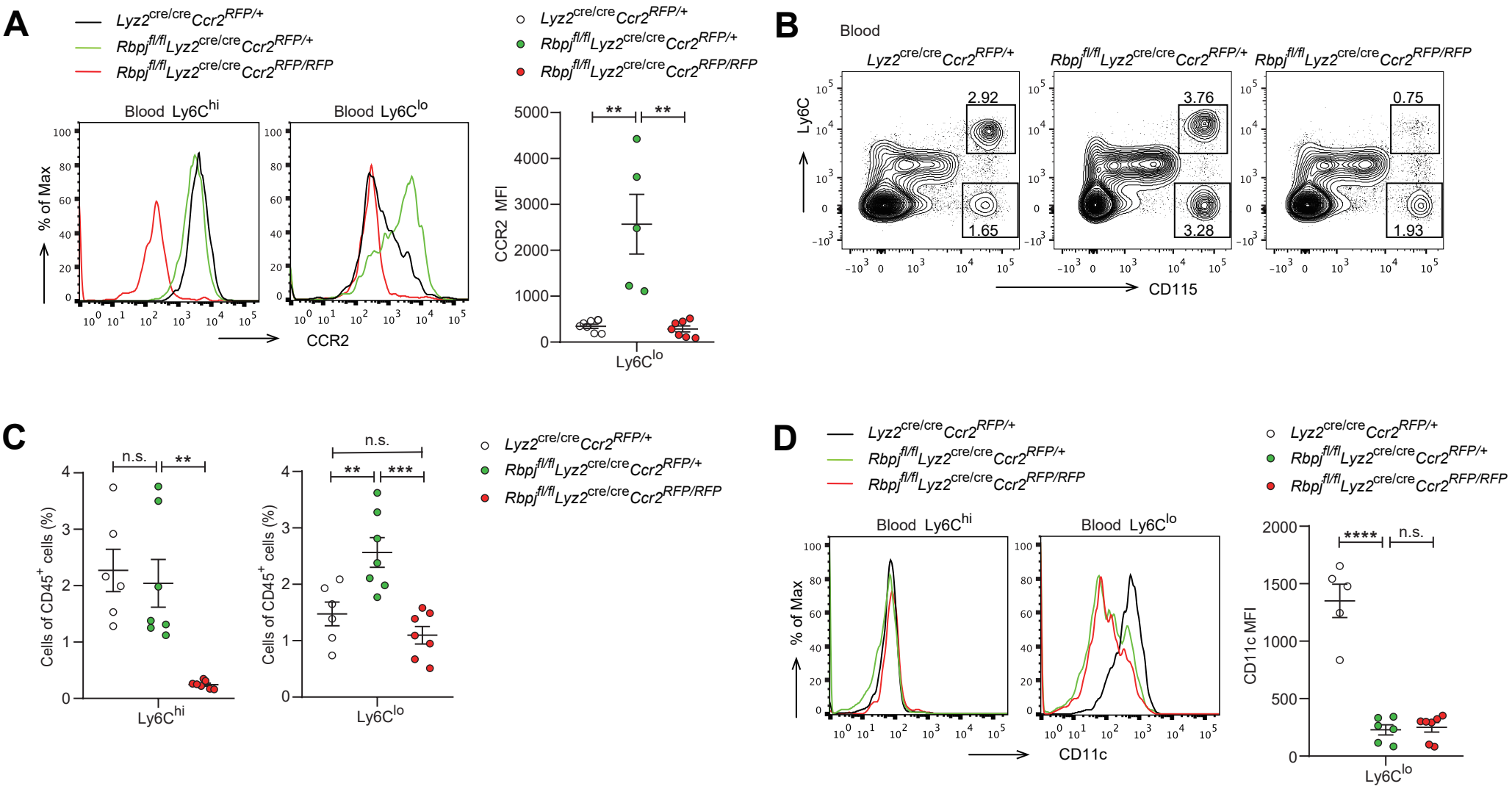
A
Lyz2cre/creCcr2RFP/+
Rbpjfl/flLyz2cre/creCcr2RFP/+
Rbpjfl/flLyz2cre/creCcr2RFP/RFP
Blood Ly6Chi
Blood Ly6Clo
% of Max
CCR2
CCR2 MFI
Ly6Clo
B
Blood
Ly6C
CD115
2.92
1.65
3.76
3.28
0.75
1.93
C
Cells of CD45+ cells (%)
Ly6Chi
Ly6Clo
n.s.
D
CD11c
CD11c MFI

Figure 5

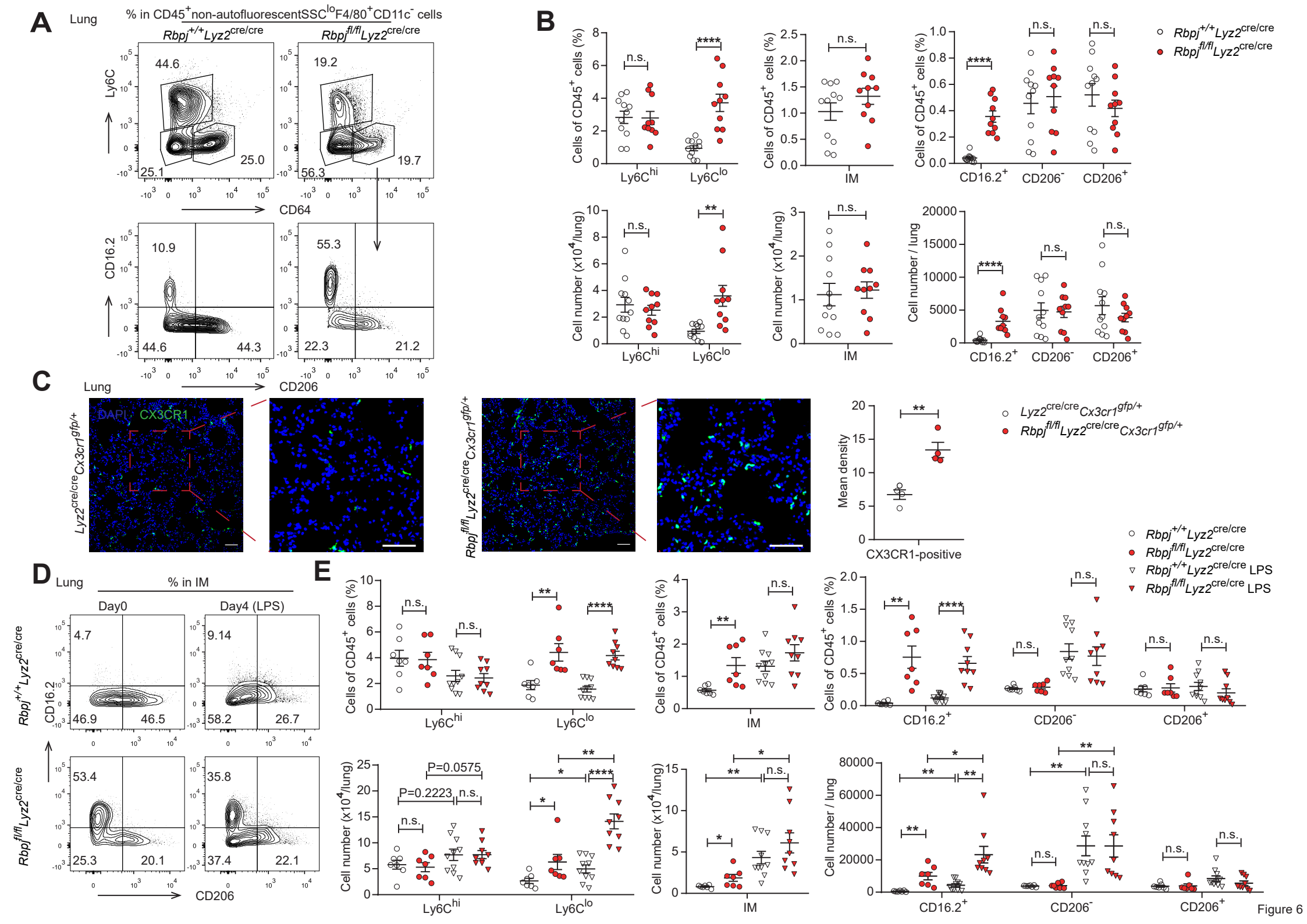
A
Lung
% in CD45+non-autofluorescentSSCloF4/80+CD11c- cells
Rbpj+/+Lyz2cre/cre
Rbpj fl/flLyz2cre/cre
Ly6C
CD64
CD16.2
CD206
44.6
25.0
25.1
19.2
19.7
56.3
10.9
44.6
44.3
55.3
22.3
21.2
B
Cells of CD45+ cells (%)
Cell number (x10^4/lung)
Cell number / lung
Ly6Chi
Ly6Clo
IM
CD16.2+
CD206-
CD206+
n.s.
****
**
C
Lung
DAPI
CX3CR1
Lyz2cre/creCx3cr1gfp/+
Rbpj fl/flLyz2cre/creCx3cr1gfp/+
Mean density
CX3CR1-positive
D
Lung
% in IM
Day0
Day4 (LPS)
4.7
46.9
46.5
9.14
58.2
26.7
53.4
25.3
20.1
35.8
37.4
22.1
E
Rbpj+/+Lyz2cre/cre LPS
Rbpj fl/flLyz2cre/cre LPS
P=0.0575
P=0.2223

Figure 6

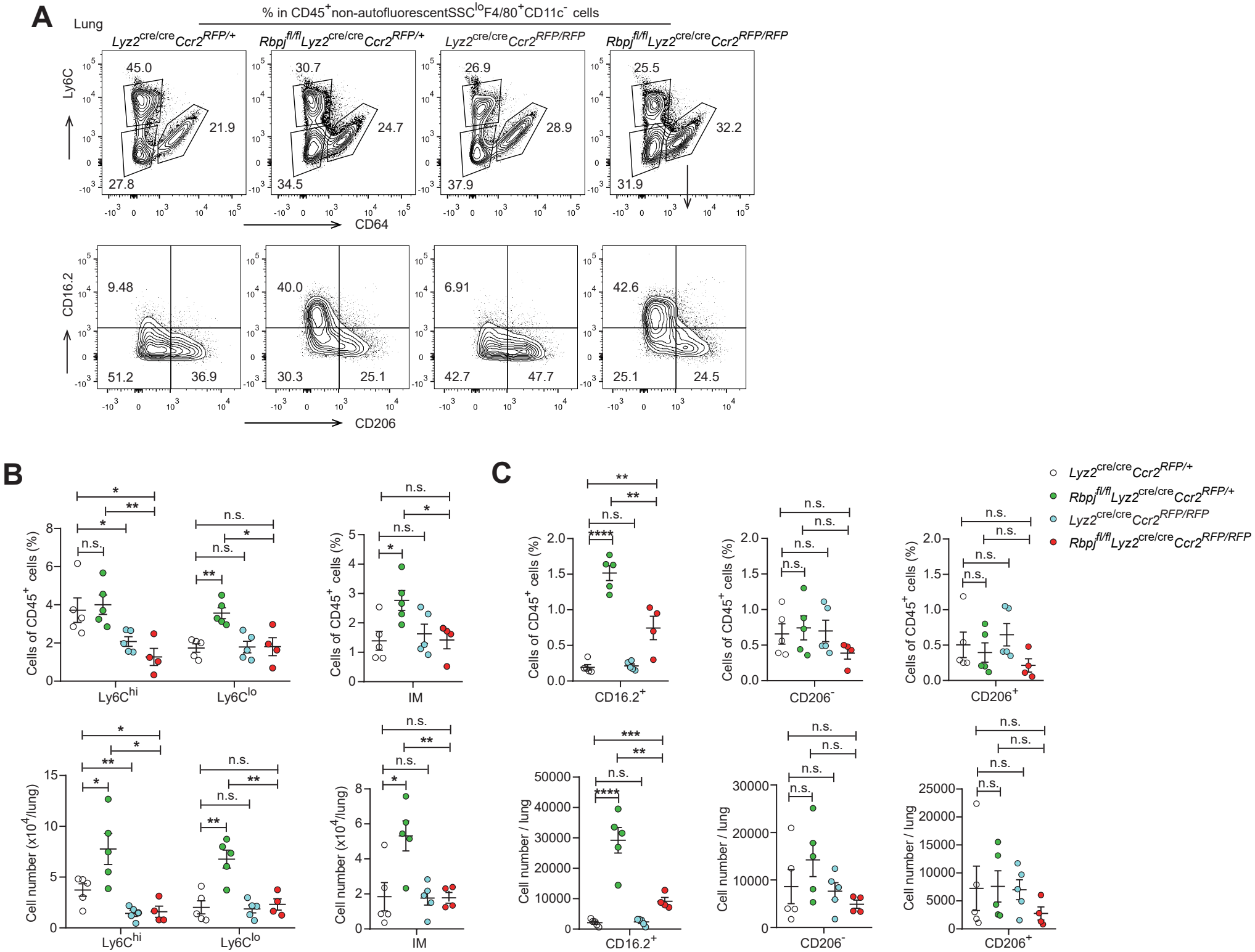
A
Lung
% in CD45+non-autofluorescentSSCloF4/80+CD11c- cells
Lyz2cre/creCcr2RFP/+
Rbpjfl/flLyz2cre/creCcr2RFP/+
Lyz2cre/creCcr2RFP/RFP
Rbpjfl/flLyz2cre/creCcr2RFP/RFP
Ly6C
CD64
CD16.2
CD206
B
C
Cells of CD45+ cells (%)
Cell number (x10^4/lung)
Cell number / lung
Ly6Chi
Ly6Clo
IM
CD16.2+
CD206-
CD206+
n.s.

Figure 7

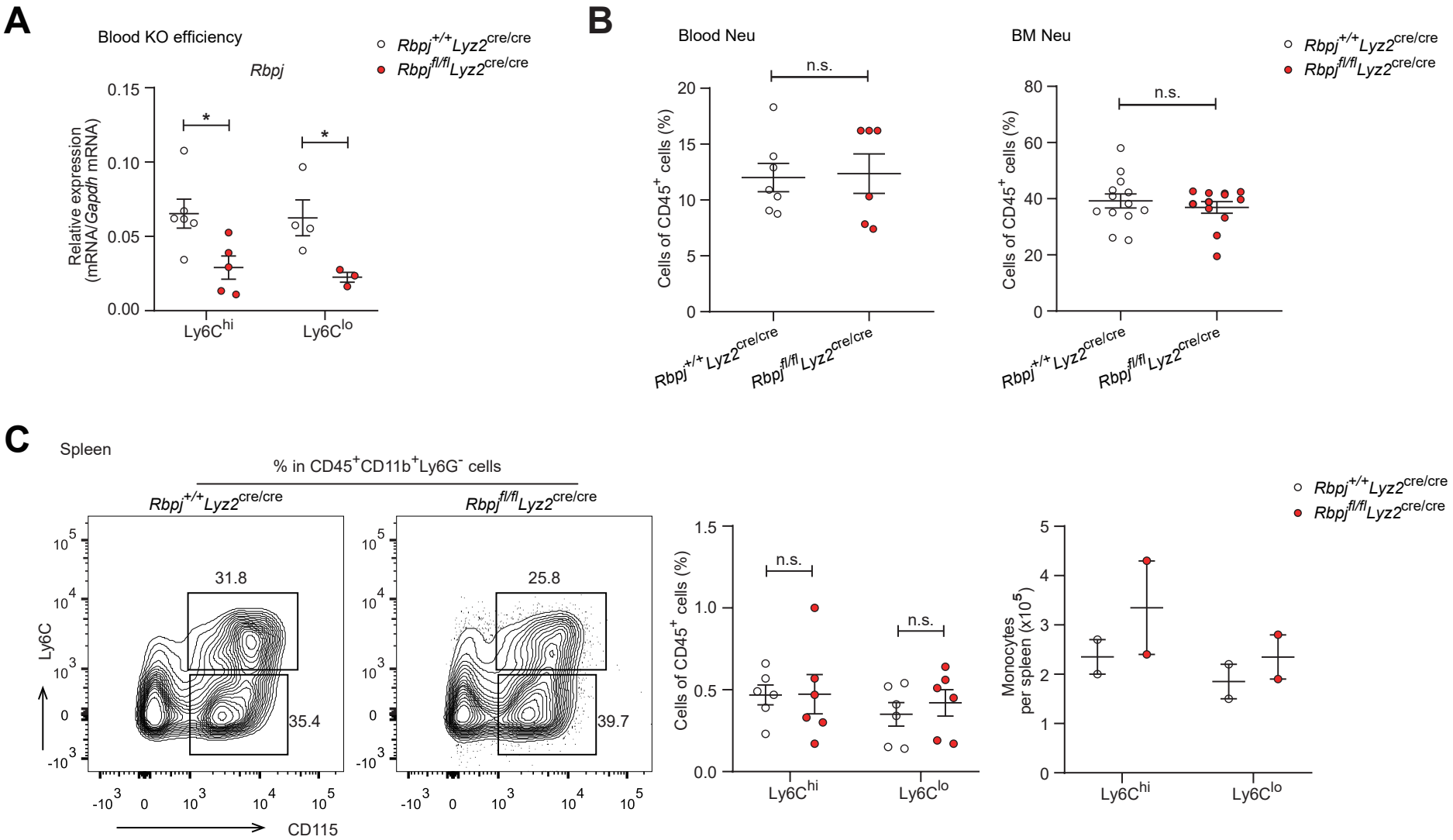


Figure 1- figure supplement 1

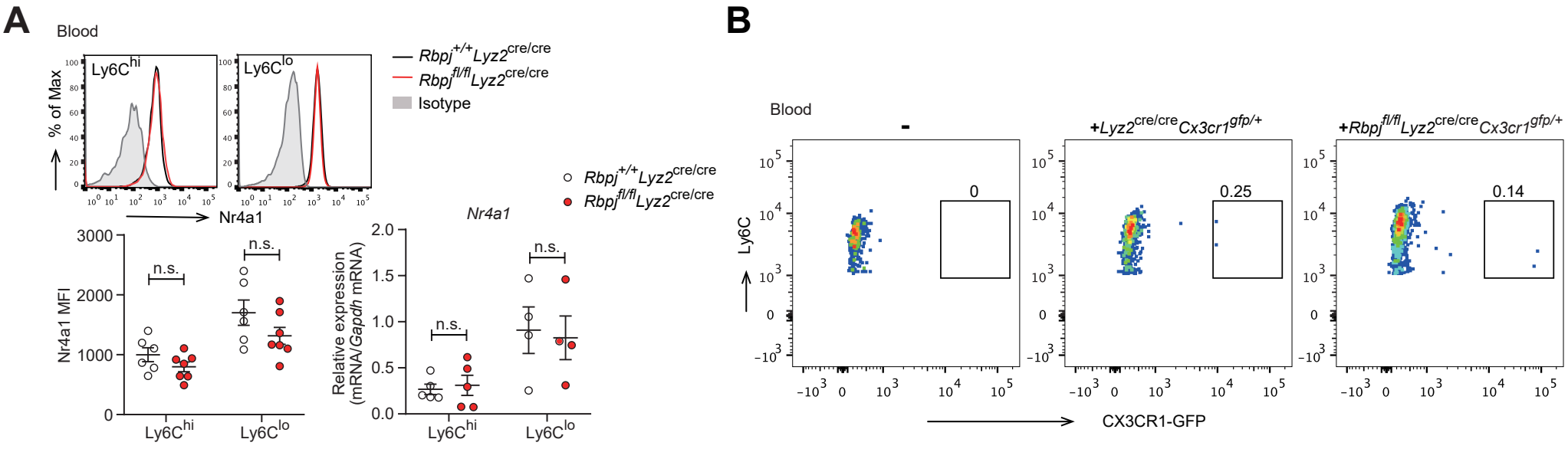


Figure 2- figure supplement 1

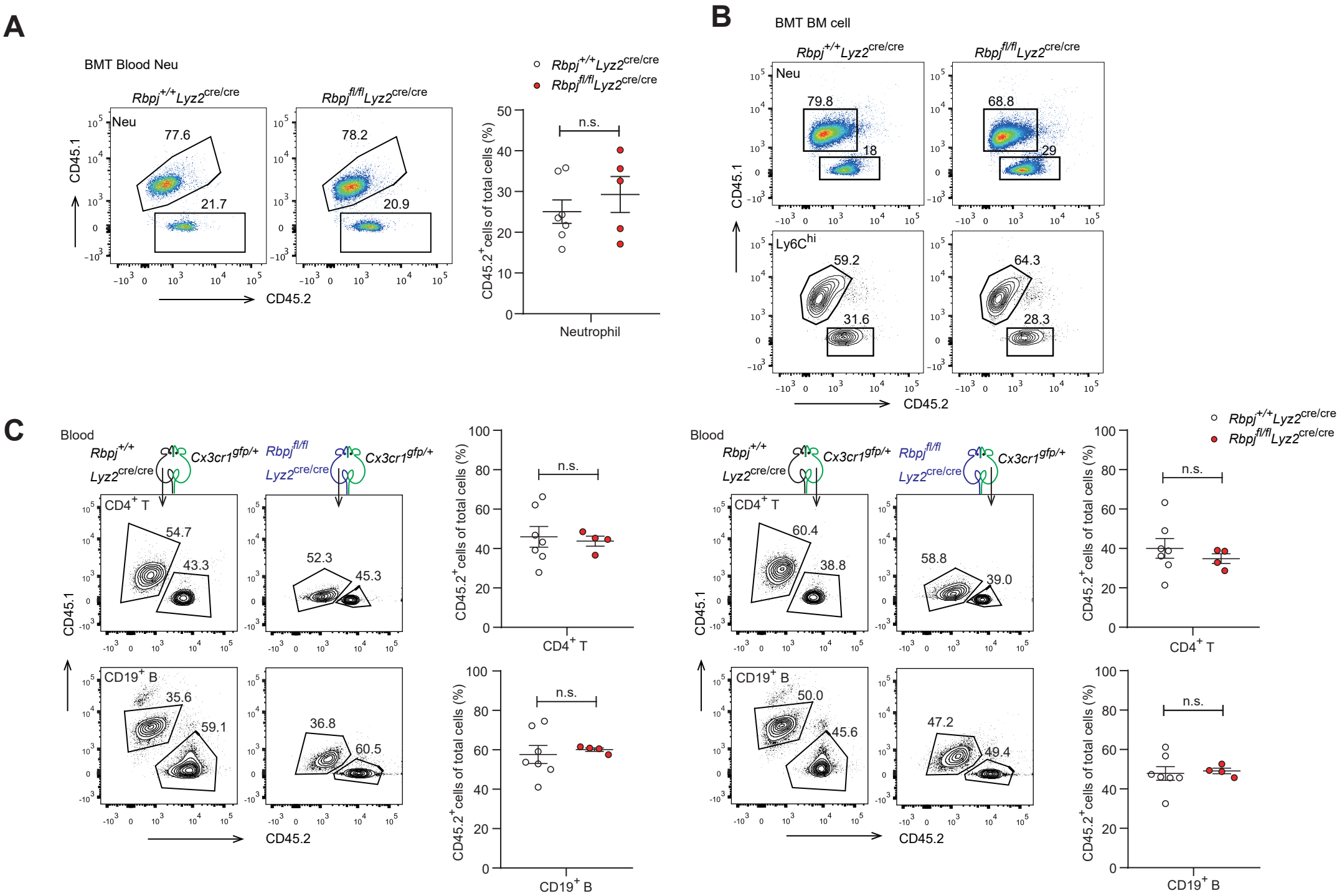


Figure 3- figure supplement 1

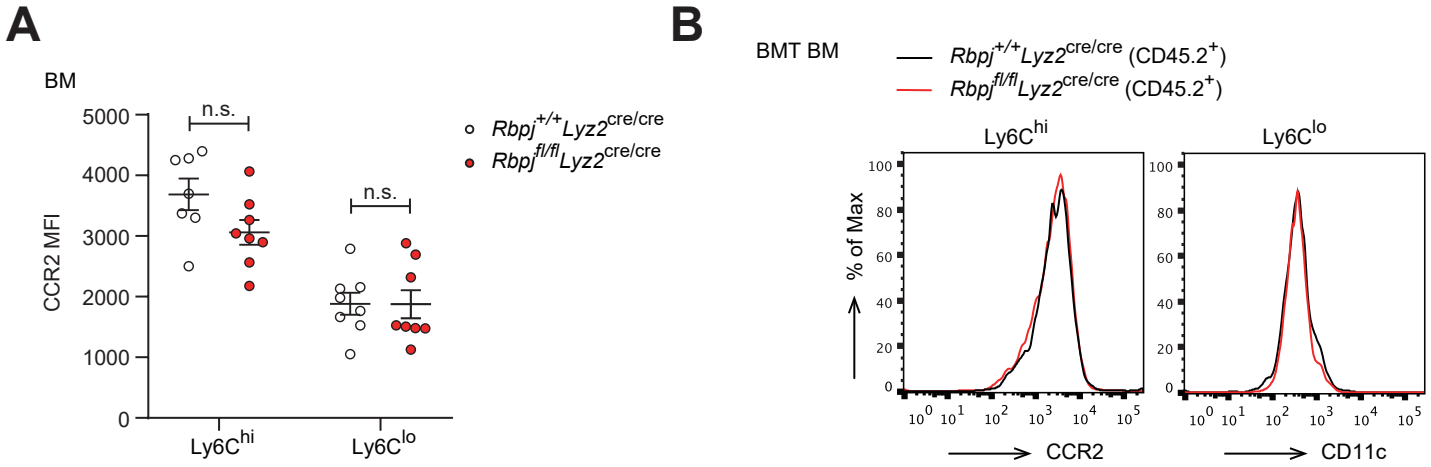


Figure 4- figure supplement 1

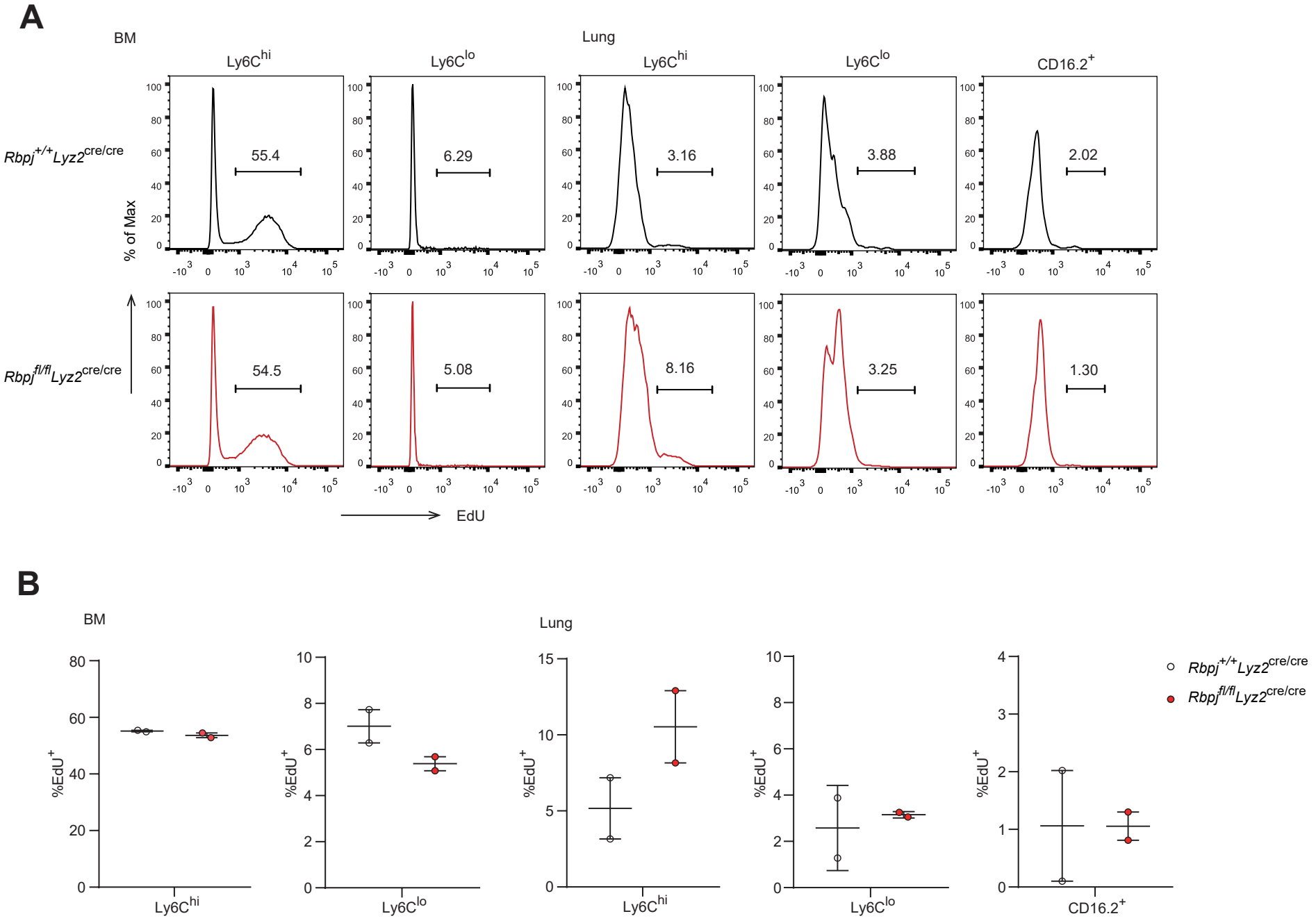


Figure 6- figure supplement 1

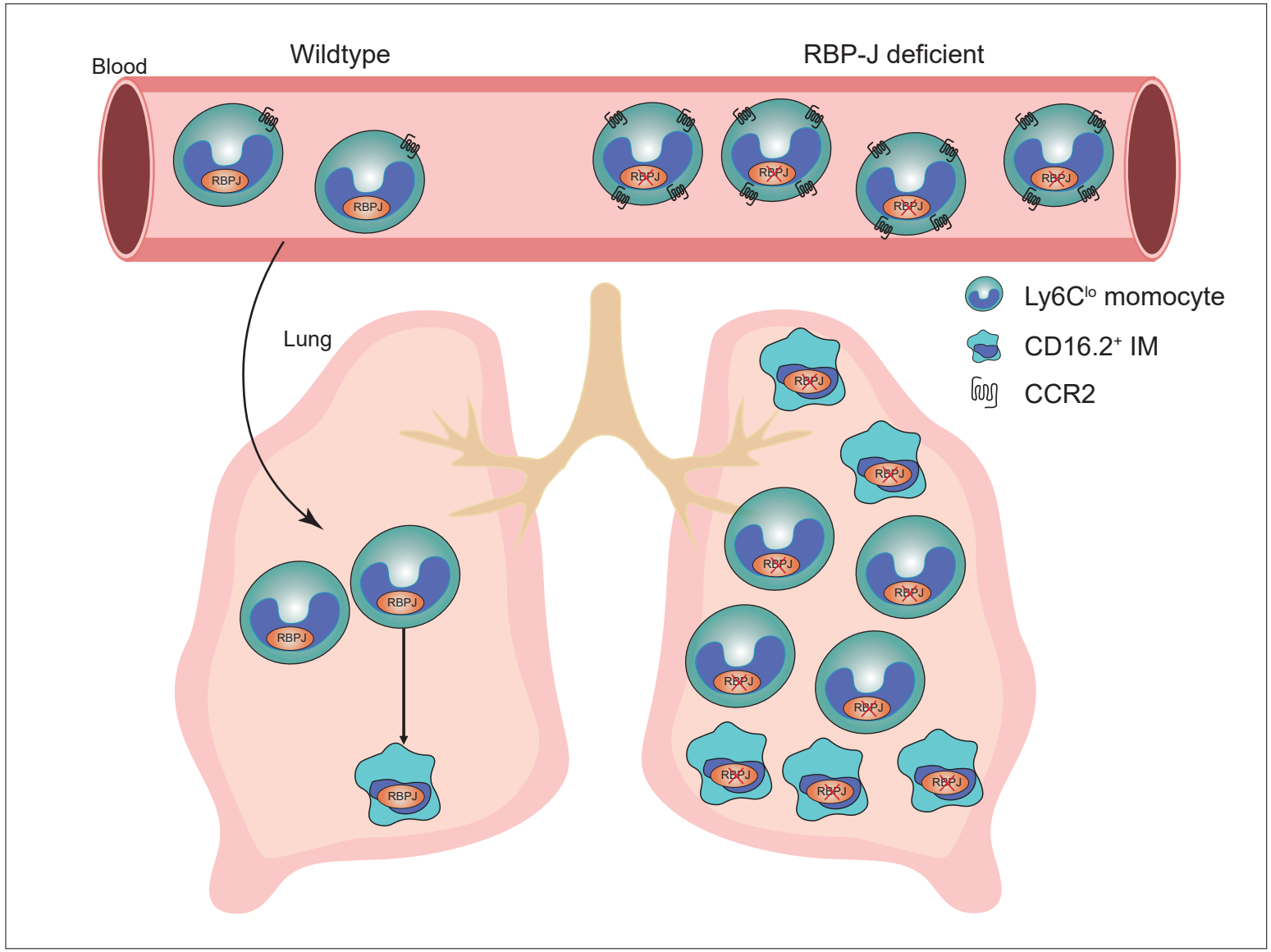


Supplementary Figure 7